

**T.R.**  
**GEBZE TECHNICAL UNIVERSITY**  
**GRADUATE SCHOOL OF NATURAL AND APPLIED SCIENCES**

**ZINC-IRON CO-DOPED/UNDOPED HYDROXYAPATITE THIN  
FILM DEPOSITION ON SILICON WAFER BY SOL-GEL METHOD**

**GÖZDE ÖCAL**  
**A THESIS SUBMITTED FOR THE DEGREE OF**  
**MASTER OF SCIENCE**  
**DEPARTMENT OF MATERIAL SCIENCE AND ENGINEERING**

**GEBZE**

**2019**

**T.R.**  
**GEBZE TECHNICAL UNIVERSITY**  
**GRADUATE SCHOOL OF NATURAL AND APPLIED SCIENCES**

**ZINC-IRON CO-DOPED/UNDOPED**  
**HYDROXYAPATITE THIN FILM**  
**DEPOSITION ON SILICON WAFER BY**  
**SOL-GEL METHOD**

**GÖZDE ÖCAL**

**A THESIS SUBMITTED FOR THE DEGREE OF**  
**MASTER OF SCIENCE**  
**DEPARTMENT OF MATERIAL SCIENCE AND**  
**ENGINEERING**

**THESIS SUPERVISOR**  
**PROF. DR. AHMET YAVUZ ORAL**

**GEBZE**  
**2019**

**T.C.**  
**GEBZE TEKNİK ÜNİVERSİTESİ**  
**FEN BİLİMLERİ ENSTİTÜSÜ**

**ÇİNKO-DEMİR BİRLİKTE**  
**KATKILI/KATKISIZ HİDROKSİAPATİT**  
**İNCE FİLMLEİN SİLİSYUM ALTLIKLAR**  
**ÜZERİNE SOL-GEL YÖNTEMİ İLE**  
**KAPLANMASI**

**GÖZDE ÖCAL**  
**YÜKSEK LİSANS TEZİ**  
**MALZEME BİLİMİ VE MÜHENDİSLİĞİ ANABİLİM DALI**

**DANIŞMANI**  
**PROF. DR. AHMET YAVUZ ORAL**

**GEBZE**  
**2019**

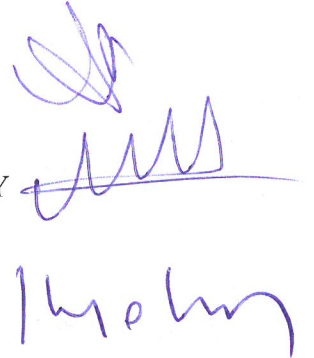
GTÜ Fen Bilimleri Enstitüsü Yönetim Kurulu'nun 03/07/2019 tarih ve ...../..... sayılı kararıyla oluşturulan jüri tarafından 12/07/2019 tarihinde tez savunma sınavı yapılan Gözde Öcal'ın tez çalışması Malzeme Bilimi ve Mühendisliği Anabilim Dalında YÜKSEK LİSANS tezi olarak kabul edilmiştir.

**JÜRİ**

ÜYE  
(TEZ DANIŞMANI) : PROF.DR. AHMET YAVUZ ORAL

ÜYE : DR.ÖĞR.ÜYESİ ALİGÜL BÜYÜKAKSOY

ÜYE : PROF. DR ERSİN KAYAHAN



**ONAY**

Gebze Teknik Üniversitesi Fen Bilimleri Enstitüsü Yönetim Kurulu'nun  
...../...../..... tarih ve ...../..... sayılı kararı.

## SUMMARY

The aim of this research is to develop zinc-iron co-doped antibacterial/antibiofilm coatings that have no harmful effects on the human body in order to prevent infection-related deaths. In the study, it is aimed to test the antibacterial / antibiofilm properties of the surfaces in biocompatibility, antibacterial efficiency and doping fields. To be able to make this analysis as a base material, it was worked with silicon wafer which do not harm health. It is widely used as an electronic material. The objectives to be reached in this study are such as; the production efficiency of zinc-iron doping in various amounts, production of antibacterial / antibiofilm coatings on a laboratory scale, investigating in-vitro biocompatibility of the produced biomaterial and testing of antimicrobial properties of biocompatible biomaterials. In this experiment, n-type with the plane direction of (100) silicon wafers were used as the base material, Hydroxyapatite (HAP) was used as the biomaterial, zinc and iron were used as doping elements to increase the bio-efficiency. It is aimed to give antibacterial properties to HAP by using these materials as non-destructive biocompatible materials. After the preparation of zinc and iron doped HAP sol-gel solutions, thin film coatings were applied on a single crystal silicon wafer substrate by dip coating method. The effects of varying amounts of zinc and iron additive on HA particle size were investigated morphologically, structural and chemically. Thin film characterization was analyzed by using Rigaku D-max RINT 2200 brand diffractometer (XRD), Philips XL 30 SFEG brand Scanning Electron Microscopy (SEM) and Energy Distributed Spectroscopy (EDS). Then, biocompatibility of the coatings which were kept in artificial body fluid for 10 days were observed by SEM analysis. Finally, the samples were tested in *Staphylococcus Aureus* bacteria medium for one week by antibacterial test.

**Key Words: Antibacterial/Antibiofilm, Hydroxyapatite, Dip-Coating, Sol-gel, Biocompatibility.**

## ÖZET

Bu deneyin amacı; insan vücudunda enfeksiyon nedeniyle oluşan ölümlere sebep olmayan çinko ve demir ile katkılanmış antibakteriyel/antibiyofilmlerin geliştirilmesidir. Bu çalışmada, antibakteriyel/antibiyofilmlerin biyoyumluluk, antibakteriyel verimliliği ve katkılandırma özelliklerinin test edilmesi amaçlanmıştır. Bu analiz yapılırken ana malzeme olarak sağlığa zararı olmayan ve elektronik malzeme olarak oldukça yaygın olarak kullanılan tek kristalli silisyum altlıklar tercih edilmiştir. Bu çalışmada ulaşılabilecek hedefler; farklı miktarlardaki çinko-demir katkı Hidroksiapatit ince film kaplamalarının üretim verimliliği, laboratuvar koşullarında antibakteriyel /antibiyofilm kaplamalarının üretimi, üretilen biyomalzemelerin in-vitro biyoyumluluğunun araştırılması ve antibakteriyel özelliklerinin test edilmesidir. Bu deneyde, tek kristalli silisyum altlıklar (n tipi) temel ince film kaplama yüzeyi olarak kullanılmıştır. Hidroksiapatit (HAP) biyomalzeme olarak; çinko ve demir ise katkı malzemesi olarak biyo-verimliliği arttırmak için kullanılmıştır. Bu malzemeleri zararsız biyoyumlu malzemeler olarak kullanarak HAP'a antibakteriyel özellikler kazandırılması amaçlanmaktadır. Çinko ve demir katkı HAP sol-jel solüsyonlarının hazırlanmasından sonra, ince film kaplamaları daldırma kaplama yöntemi ile tek kristalli silisyum altlık üzerine ince film kaplamaları uygulanmıştır. Değişik miktarlarda çinko ve demir katkı maddesinin HA partikül boyutuna etkileri morfolojik, yapısal ve kimyasal olarak incelenmiştir. İnce film karakterizasyonu Rigaku D-max RINT 2200 marka difraktometre (XRD), Philips XL 30 SFEG marka Taramalı Elektron Mikroskopu (SEM) ve Enerji Dağılımı Spektroskopisi (EDS) kullanılarak analiz edilmiştir. Daha sonra, yapay vücut sıvısında 10 gün boyunca tutulan kaplamaların biyoyumluluğu SEM analizi ile gözlenmiştir. Son olarak, numunelerin bir hafta boyunca *Staphylococcus aureus* bakteri ortamında antibakteriyel özelliği test edilmiştir.

**Anahtar Kelimeler: Antibakteriyel/Antibiyofilm, Hidroksiapatit, Dip-coating, Sol-jel, Biyoyumluluk.**

## ACKNOWLEDGEMENTS

First of and foremost, I would like to thank my academic advisor, Prof. Dr. Ahmet Yavuz ORAL for his guidance and encouragement with his immense knowledge and for giving me this opportunity to discover myself.

Beside my advisor, I would like to thank to Mehmet SEZER, Seda KOL, Mehmet Emre AKÖZ, Can ORAL, Adem ŞEN and Ahmet NAZIM for their contribution, collaboration and help during this time range to face each and every problem together as a wonderful team.

I am also grateful and thankful to my beloved husband Samet GÜLEÇ for his valuable support and also to my family and friends; Kardelen Afroditi Adsal and Ayten Eylül Efe who are encouraging and motivating me all the time to be able to face all my difficulties.

This study taught me that I can overcome and accomplish everything by working hard, planning and believing. From now on I promise that I will always improve and interrogate myself until my last breath.

# TABLE of CONTENTS

	<u>Page</u>
SUMMARY	v
ÖZET	vi
ACKNOWLEDGEMENTS	vii
TABLE of CONTENTS	viii
LIST of ACRONYMS and ABBREVIATIONS	x
LIST of FIGURES	xi
LIST of TABLES	xiii
1. INTRODUCTION	1
1.1. Biomaterials	1
1.1.1. Fundamental Properties of Biomaterials	4
1.1.1.1. Biocompatibility	4
1.1.1.2. Mechanical Properties	5
1.1.1.3. Osteointegration	6
1.1.1.4. Corrosion Resistance	6
1.1.1.5. Abrasion Resistance	7
1.1.2. Classification of Biomaterials	7
1.1.2.1. Metallic Biomaterials	8
1.1.2.2. Ceramic Biomaterials	11
1.1.2.3. Polymeric Biomaterials	12
1.1.2.4. Composite Biomaterials	13
1.2. Hydroxyapatite	13
1.3. Sol-Gel	17
1.3.1. Steps of Sol-Gel	19
1.3.1.1. Hydrolysis Reaction	20
1.3.1.2. Condensation Reaction	20
1.3.1.3. Polymerization	21
1.3.1.4. Gelation	22
1.3.1.5. Aging	22
1.3.1.6. Drying	22



1.3.1.7. Coating	22
1.3.2. Sol-Gel Coating of Materials	23
1.3.3. Dip Coating	25
1.4. Properties Zinc Oxide	26
1.5. Properties of Iron	28
1.6. Relation Between Bacteria-Implant and Infection	29
2. EXPERIMENTAL	31
2.1. General Overview of Zn-Fe doped HAP Process	31
2.2. Preparation of Silicon Wafers	31
2.3. Preparation of Sol-Gel, Thin Film and Heat Treatments	32
2.4. Preparation of Simulated Body Fluid (SBF)	35
2.5. Preparation of Zn-Fe co-doped HAP Powder for Particle Size Distribution and Preparation of Antibacterial Test	38
2.5.1. Particle Size Distribution	38
2.5.2. Preparation of Antibacterial Test	39
2.6. Chemical Composition, Phase Analysis and Microstructure of Thin Films	39
3. RESULTS	40
3.1. Particle Size Distribution	40
3.2. TG/DTA Analysis	41
3.3. Thin Film Microstructure Analysis X-RAY Diffraction (XRD)	43
3.4. EDS Analysis	48
3.5. SEM Analysis and Biocompatibility	50
3.6. Antibacterial Test	55
4. CONCLUSION	57
REFERENCES	58
BIOGRAPHY	67

## LIST of ACRONYMS and ABBREVIATIONS

<u>Acronyms and Abbreviations</u>	<u>Explanations</u>
°	: Degree
Θ	: Theta
μm	: Micrometer
nm	: Nanometer
β – TCP	: Whitlocite
M	: Molarity
C	: Celcius
Ca	: Calcium
CNT	: Calcium Nitrate Thetrahydrate
d	: Distance
DTA	: Differential Thermal Analysis
Fig.	: Figure
g	: Gram
h	: Hour
HAP	: Hydroxyapatite
min.	: minute
ml	: Mililiter
PA	: Polyacetal
PE	: Polyethylene
PMMA	: Poly (methyl methacrylate)
PTFE	: Polytetrafluoroethylene
PU	: Polyurethane
TG	: Thermogravimetric
ZAD	: Zinc Acetate Dihydrate

## LIST of FIGURES

<b><u>Figure No:</u></b>		<b><u>Page</u></b>
1.1:	Factors causing damage to implant material.	4
1.2:	Dimensional HAP crystal and HAP structure along the c-axis.	16
1.3:	Solubility of calcium phosphate species according to a) calcium and b) phosphate concentrations.	16
1.4:	Sol-gel process.	17
1.5:	Some of the coating methods used in the sol-gel method a) Dip coating b) Spin coating.	23
1.6:	Functionalities of materials by sol-gel method.	24
1.7:	a) Hexagonal wurtzite structure b) ZnO crystal structure.	26
2.1:	General overview of Zn-Fe doped HAP process.	31
2.2:	Silicon Wafer (100) Cleaning.	32
2.3:	Preparation of the Solution.	34
2.4:	Flow Chart of Thin Film Formation in Dip-Coating.	35
2.5:	Chemical steps, formulae and the mole of SBF.	37
2.6:	Preparation of particle size distribution analysis.	38
3.1:	Particle Size Distribution.	40
3.2:	TG Analysis of Zn-Fe co-doped HAP.	41
3.3:	DTA Analysis of Zn-Fe co-doped HAP solution.	41
3.4:	XRD Analysis of 0,0005 mole Zn-Fe doped HAP thin film.	43
3.5:	XRD Analysis of 0,001 mole Zn-Fe doped HAP thin film.	44
3.6:	XRD Analysis of 0,0015 mole Zn-Fe doped HAP thin film.	44
3.7:	XRD Analysis of 0,002 mole Zn-Fe doped HAP thin film.	45
3.8:	XRD Analysis of 0,0025 mole Zn-Fe doped HAP thin film.	45
3.9:	XRD Analysis of 0,003 mole Zn-Fe doped HAP thin film. a: HAP, b: $\beta$ -TCP (Whitlocite), c: ZnO, d: CaO	46
3.10:	Atomic dispersion of 0,0025 mole doped Zn-Fe co-doped thin film.	48
3.11:	Net intensity of 0,0025 mole doped Zn-Fe co-doped thin film.	49
3.12:	0,0005 mole Zn-Fe co-doped HAP thickness measurement.	50

3.13:	0,0005 mole Zn-Fe co-doped HAP thin film SEM images.	51
3.14:	0,001 mole Zn-Fe co-doped HAP thin film SEM images.	51
3.15:	0,0015 mole Zn-Fe co-doped HAP thin film SEM images.	52
3.16:	0,002 mole Zn-Fe co-doped HAP thin film SEM images.	52
3.17:	0,0025 mole Zn-Fe co-doped HAP thin film SEM images.	53
3.18:	0,003 mole Zn-Fe co-doped HAP thin film SEM images.	53
3.19:	Antibacterial test result of 0,003 mole Zn-Fe co-doped HAP pellet.	55



## LIST of TABLES

<b><u>Table No:</u></b>		<b><u>Page</u></b>
1.1:	The most widely used biomaterials as implants.	3
1.2:	Modulus of elasticity values of commercial alloys used in biomedical applications.	5
1.3:	Stainless Steel Medical Applications.	9
1.4:	Effects of alloying elements.	10
1.5:	General mechanical properties of titanium and its alloys developed for orthopedic implants.	11
1.6:	Important scientific developments related to HAP.	14
1.7:	Calcium phosphates and some properties.	15
1.8:	Some of the properties of ZnO at 300 K.	27
2.1:	The formulae of HAP Precursors.	33
2.2:	Iron and Zinc Formula.	33
2.3:	The total used amounts of Zinc/Iron co-doped HAP solution.	34
3.1:	Elemental analysis of 0,0025 mole doped Zn-Fe co-doped thin film.	49

# 1. INTRODUCTION

The material used in the treatment of organs and tissues that are lost or damaged due to accidents or diseases in the human body is called “Biomaterials”. With the development of technology, the importance and application area of biomaterials are increasing. Today, biomaterials are used in dental implants, hip prostheses and in the production of nanoscale biorobots. Biomaterials are biocompatible because they are in constant or periodic contact with the body fluid. Biocompatibility is defined as surface and structural compatibility. Structural compatibility is the optimal adaptation of biomaterial to the mechanical behavior of body tissues. Surface compatibility means that the material is chemically biologically and physically suitable for body tissues.

First part of this study; biomaterials, biocompatibility, interactions of biomaterials with the body, structure of Hydroxyapatite, Hydroxyapatite properties, Hydroxyapatite production methods, sol-gel and dip coating methods were reviewed.

In the last part of the study; Zinc-Iron co-doped Hydroxyapatite thin films and powders were investigated in Thermogravimetric Analysis, Differential Thermal Analysis and Antibacterial Test. The doped Hydroxyapatite thin film was coated on silicon wafer (n, 100) and characterized; X-ray Diffraction Diffractometer (XRD), Scanning Electron microscope (SEM) and Energy Dispersive Spectrometer (EDS). Differences caused by changes in the amount of additives were examined.

## 1.1. BIOMATERIALS

Biomaterials are the name of materials that are used to fix the functional losses caused by tissue damage and tissue loss. Biomaterials can be natural or synthetic. According to European Biomaterial Community, a biomaterial can replace body functions, tissues and organs, undertake healing, growth and repair tasks and interact with biological systems by interfacing. As biomaterial; contact lenses, prostheses used in the field of orthopedics, dental fillings, artificial cornea can be given as examples [1].

Biomaterials can be produced from different materials (ceramic, polymer, metal and composite);

- To support aesthetic appearance (skin implementations, braces, silicone)
- Improve functionality (lens, pacemaker, hearing aid),
- Helping treatment (catheter, drainage),
- Helping recovery (surgical thread, screw and wire),
- Replacement of damaged or diseased parts of the body (dialysis, prostheses),
- Assist in the diagnosis of the disease (biosensors, endoscopy, injector),
- Correcting dysfunction (spine fixators)

Are various uses of biomaterials [2,3].

The use of biomaterials dates back to ancient times. The artificial eyes, nose and teeth found in Egyptian mummies are the most primitive examples of implants. Evidence of the use of gold in dentistry until 2000 years ago and evidence for the use of bronze and copper bone implants goes back to BC [4]. In the early 1900s, bone plates were used to support the fixation of long bone fractures. Many of the bone plates used were broken due to their very thin and incorrect mechanical design, such as having high density corners. Furthermore, these bone plates are made of vanadium steels due to their good mechanical properties, but their rapid deterioration in the body adversely affected the healing process. The first successful joint replacement operation was performed in the 1930s using stainless steel and cobalt-chromium alloys [5].

Since no side effects or inflammation occurred in the fighter pilots who were injured with polymethyl methacrylate (PMMA) during the Second World War, PMMA material was used to replace corneal and damaged skull bones. Following the development of materials and surgical techniques, blood vessel prosthesis was developed in the 1950s and heart valve prosthesis was developed in the 1960s. [5]. Although alumina and zirconia used in the 1970s because they did not cause any biological negativity, this problem was solved [4]. These developments continued with the “Nanomaterials” developed in the field of “Tissue Engineering” and biomaterials in the 2000s.

Table 1.1: The most widely used biomaterials as implants.

APPLICATION FIELD	MATERIAL TYPE
<b>Skeleton System</b>	
Knuckles	Titanium, Titanium-Aluminum-Vanadium alloys
Thin metal sheets used for determination of broken bone ends	Stainless steel, cobalt-chrome alloys
Bone filler	Poly (methyl methacrylate) (PMMA)
Treatment of bone deformities	Hydroxyapatite
Artificial tendons and ligaments	Teflon, poly (ethylene terephthalate)
Dental implants	Titanium, alumina, calcium phosphate
<b>Cardiovascular System</b>	
Blood vessel prostheses	Poly (ethylene terephthalate), teflon, polyurethane
Heart valves	Stainless steel, carbon
The catheters	Silicone Rubber, Teflon, Polyurethane
<b>Organs</b>	
Artificial heart	Polyurethane
<b>Sense organs</b>	
Inner ear canal	Platinum electrodes
Intraocular lenses	PMMA, silicone rubber, hydrogels
Contact lenses	Silicone-acrylate, hydrogels
Corneal bandage	Collagen, hydrogels

Biomaterials used as an implant from past to present and their application areas are given in the Table 1.1 [4].

The long-term use of biomaterials in the body depends on the material properties, the design of the material, the biocompatibility of the material (compatibility with the body), the condition of the patient, and the technique used by the surgeon [6]. Biomaterials suffer damage when they are not designed properly to meet the requirements of their place of use, requiring a new surgery. The most common factors for damage to an implant material are shown schematically in Figure 1.1 [7].



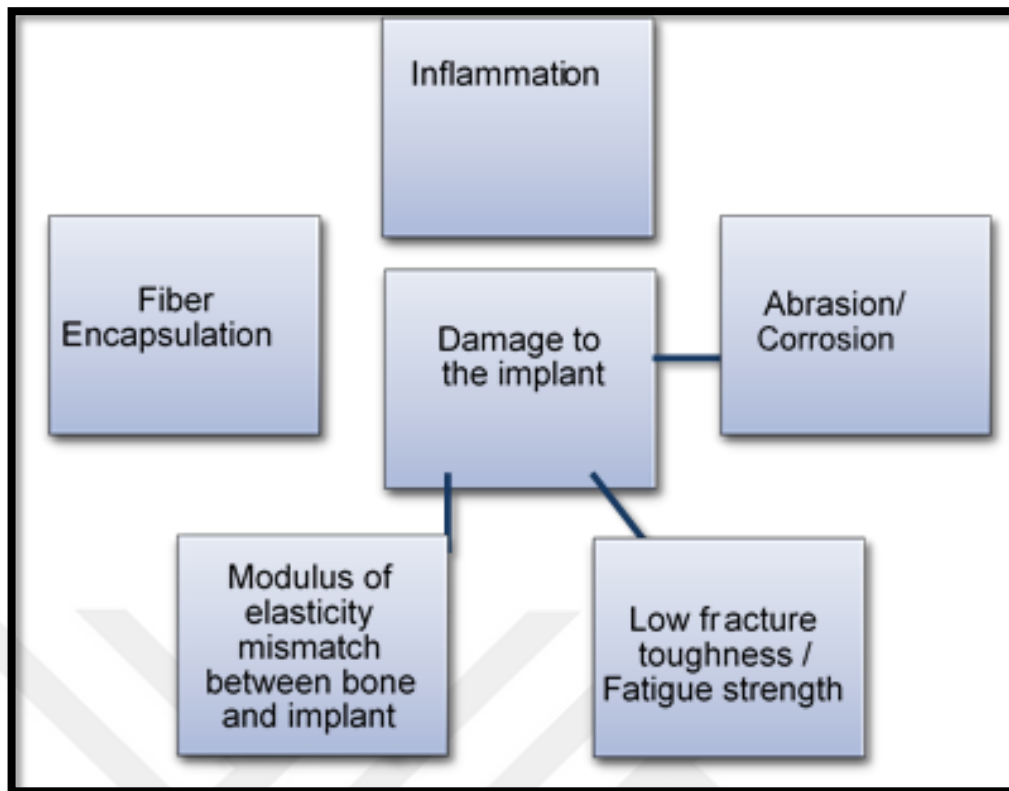


Figure 1.1: Factors causing damage to implant material.

### 1.1.1. Fundamental Properties of Biomaterials

In order to apply biomaterials smoothly and to be used for a long time, it needs to meet certain needs of the human body. These needs are; biocompatibility, osteointegration, mechanical properties, corrosion resistance and abrasion resistance [8].

#### 1.1.1.1. Biocompatibility

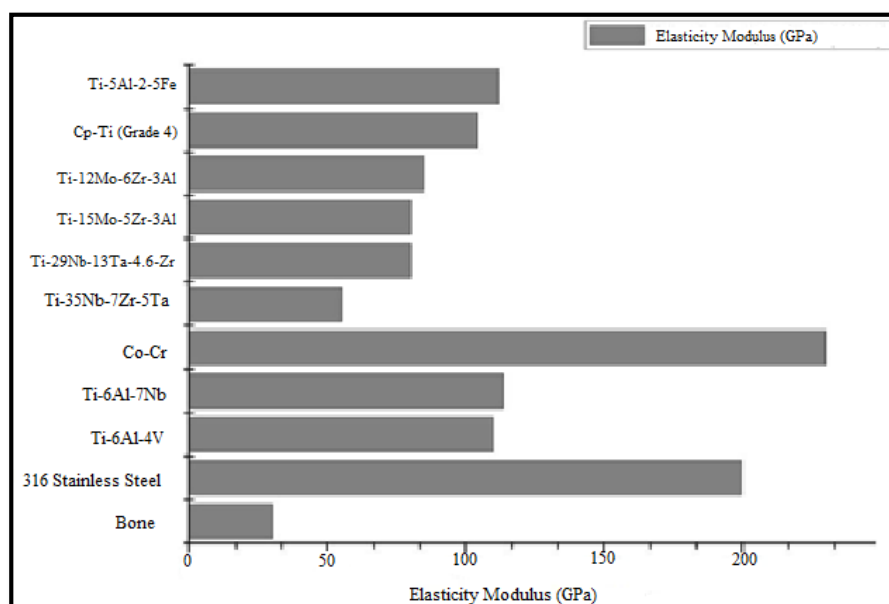
The problem-free use of biomaterials depends on the reaction of the human body with the implant material. Biomaterials used as implants are expected to show no allergic reactions in the human body and not toxic [8]. The ability of the material to respond appropriately to the body system is defined as biocompatibility [9]. There are two main factors affecting the biocompatibility of the material; the first is the reaction of the material to the body and the second is the degradation of the material

in the body. According to the response to the human body, biomaterials are grouped as; bioinert, bioactive and biodegradable [10].

### 1.1.1.2. Mechanical Properties

Among the mechanical properties of biomaterials, primary properties are hardness, tensile strength, modulus of elasticity (E) and elongation. False mechanical strength of the implant and damage to the implant due to the modulus of elasticity mismatch between the implant and bone tissue is called biomechanical incompatibility. For this reason, the modulus of elasticity of the implant material to be used in place of the bone should be equivalent to the bone [8]. For example, the elasticity modulus of the Co-Cr alloy is around 210–253 GPa, while the elasticity modulus of the bone is in the range of 4 to 30 GPa depending on the loading direction and the type of bone. Due to the high modulus of elasticity, an inhomogeneous stress shielding occurs between the bone and the implant. This causes the implant and surrounding bone to corrode, preventing bone and implant from fusing. Elasticity modulus values of commercial metal alloys used as biomaterials are given schematically in Table 1.2 [7].

Table 1.2: Modulus of elasticity values of commercial alloys used in biomedical applications.



### **1.1.1.3. Osteointegration**

The term osteointegration was first used by Branemark in 1983 to describe the bond between the bone and the titanium surface. Attachment of living tissue and implant is called osteointegration [9,11]. Inadequate interaction of the implant with the bones and tissues leads to implant losses. The occurrence of osteointegration depends on the initial contact of the implant surface with the body, so surface chemistry, surface roughness and surface topography of the implant play an important role. The good integration of the bone tissue and the implant significantly affects the efficiency and life of the implant [11]. For example, titanium materials are of great importance in terms of surface properties and bone-implant interaction. However, the percentage of bone-titanium integration ( $\leq 65\%$ ) is well below the ideal (100%) [12]. Bioactive materials have been developed to solve surface integration problems. These materials form a unique biological bond that can act as natural tissues and prevent movement between the implant and tissue at the interface. In this way, bone formation occurs between materials and tissues. Examples of materials in this group are Hydroxyapatite, Bio Glass, Glass-ceramics and coatings made with these materials [4].

### **1.1.1.4. Corrosion Resistance**

Corrosion is the degradation of metals and alloys as a result of their chemical and electrochemical interactions with their environment. Corrosion of metallic implants is important because it negatively affects biocompatibility and mechanical integrity. For this reason, the biomaterial use should not cause a biological reaction that would have a negative effect on the body and should be a stable material that retains its functional properties in the body fluid [12,13].

The human body contains different pH values and different oxygen concentrations. In addition, there are various anions and cations dissolved in the body fluid to accelerate the corrosion. Under normal conditions, the human body fluid is composed of approximately 0.9% saline, mostly  $\text{Na}^+$ ,  $\text{Cl}^-$  ions, amino acids and water-soluble proteins. Therefore, although the implant material performs well in

environmental conditions, it may be exposed to a high degree of corrosion within the body [12,13].

Implant materials that are corroded over time lead to ion release. The released ions damage the bone and surrounding tissue. In addition, low corrosion resistance of the implant affects its mechanical properties such as fatigue life and pull strength negatively. Therefore, it is essential to protect the implant material from corrosion [12]. The corrosion behavior of the material depends largely on the passive protective oxide layer it forms. The protective effect of the passive layer reduces both the corrosion rate and ion release of the material. Furthermore, since the formed passive oxide layer will be in direct contact with the biological tissue, the characterization of the surface composition is also very important [14]. For instance, the TiO<sub>2</sub> oxide layer formed on the surface of titanium has significantly improved corrosion resistance [15].

#### **1.1.1.5. Abrasion Resistance**

Abrasion is referred to as surface damage involving a continuous loss of material due to movement between two materials in contact with each other [12]. Abrasion is an inevitable problem in every joint prosthesis regardless of the type of material [13]. Low wear resistance can lead to implant losses and stored wear residues can cause tissue reactions [8].

Skeletal system contains; hip, shoulder, knee, and more stable teeth, skull and ankle joints. The choice of implant material varies according to the type of joint. Especially with ceramic biomaterials used in mobile joints such as hip, knee and ankle, the abrasion rate is reduced, and the amount of ion release is decreased to negligible levels. Metallic or hard polymeric materials are preferred for more stable joints such as teeth, wrists and skulls [13].

## **1.1.2. Classification of Biomaterials**

Biomaterials are divided into two groups as artificial and natural biomaterials (gelatin, collagen, chitin, chitosan). Artificial biomaterials can be classified under 4 main groups;

- Metallic biomaterials,
- Ceramic biomaterials,
- Polymeric biomaterials
- Composite biomaterials

### **1.1.2.1. Metallic Biomaterials**

Metallic biomaterials have disadvantages such as low biocompatibility, corrosion, being very hard to tissues, high densities, and metal ion release that can cause allergic tissue reactions. However, despite these disadvantages, metals and alloys having superior mechanical properties with crystal structures and very strong metallic bonds; It is one of the materials that best adapt to the mechanical conditions of our musculoskeletal system [9,16]. Therefore, metallic biomaterials constitute approximately 70% of all biomaterials [7].

Metallic biomaterials used as heart parts, catheters, valves, heart valves in orthopedic applications, face and jaw surgery (eg dental implant) and cardiovascular surgery as joint prosthesis and bone replacement material [7].

Metallic biomaterials can be classified according to pure metal or alloy elements in 3 different ways. These; stainless steels, Co-Cr alloys, titanium and titanium alloys. Ni-Ti alloy, also known as shapee memory alloys, is an example of metallic biomaterials [7].

Stainless steel is the general name for iron-based steels with varying amounts of nickel and a high proportion (11 to 30 wt%) of chromium. Stainless steels are classified as martensitic, ferritic, austenitic and duplex steels according to microstructures. Other stainless steels other than duplex stainless steel are used in medical applications (Table 2.2) [13]. Austenitic stainless steel 316 and 316L are the

most commonly used types of stainless steel as implants [5]. The material type, applications and the examples of metallic biomaterials are shown at below Table 1.3.

Table 1.3: Stainless Steel Medical Applications.

Material Type	Application Class	Examples
Martensitic	Dental and surgical instruments	Orthodontic pliers and scalpel.
Ferritic	Some surgical instruments	Guide pins, connection elements
Austenitic	Numerous non-implantable medical devices	Guide pins, hypodermic needles, injection syringes
Duplex	Not used in biomedical area	

The first metallic biomaterial made of stainless steel is an 18/8 Cr / Ni stainless steel implant. This type of biomaterials is made of Vanadium steel because of its durability and high corrosion resistance. Since the corrosion resistance of vanadium steel in the body is insufficient, it is not suitable for long-term use as an implant. To eliminate this disadvantage, the Mo% of 18/8 s Mo stainless steel was increased slightly and the corrosion resistance of the alloy increased against the brine solution. This alloy is known as ASTM 316 (American Society for Testing and Materials) stainless steel. In 1950, the carbon (C) in 316 stainless steel was reduced from 0.08% to 0.03% and the corrosion resistance of the alloy showed better results in brine solution. C ratio reduced to 0.03% 18/8 CrNi stainless steel is called ASTM 316 L steel [5].

The main alloying element affecting the corrosion resistance of stainless steels is Cr' and the amount of Cr must be at least 11%. Chromium is an inactive element. However, pure Cr and its alloys are formed by the active but protective chromium oxide layer on the material surfaces. Austenitic 316 and 316L type alloys can't be hot-cured, but cold-curing can be applied to these materials. This group of stainless steels is non-magnetic and has high corrosion resistance in-vivo than other stainless steels. By adding Mo to the alloy, the alloy's resistance to pitting corrosion in the brine environment is increased. Therefore, ASTM recommends 316 L stainless steel more than 316 stainless steel for use as biomaterial [5].

Two types of cobalt-chromium (Co-Cr) alloys are used in the field of biomaterials. These; casting CoCrMo and forged CoNiCrMo alloys. CoCrMo alloys are used in dentistry and in newly developed artificial joints. CoNiCrMo alloy is used as a prosthetic stem material in hip and knee joints carrying heavier loads than CoCrMo alloys (Park and Lakes, 2007).

ASTM divided CoCr alloys into 4 groups according to their applications in the field of surgery. These; CoCrMo (F75), CoCrWNi (F90), CoNiCrMo (F562), CoNiCrMoWFe (F563) are alloys [5]. Co-Cr based alloys exhibit higher corrosion resistance than stainless steels in environmental conditions which contain chlorine ions such as sea water due to their chemical composition. The effects of Cr and other alloying elements used are indicated in Table 1.4 [13].

Table 1.4: Effects of alloying elements.

Elements	Effects on corrosion resistance	Effects on microstructure	Effects on mechanical properties
Cr	Creates a passive oxide layer of Cr <sub>2</sub> O <sub>3</sub>	Creates Cr <sub>23</sub> C <sub>6</sub>	Improves abrasion resistance
Mo	Increases corrosion resistance	Grain Thin	Solid melt strengthening
Ni	Increases corrosion resistance		Solid melt strengthening, Increases pourability
W	Reduces corrosion resistance	Reduces shrinkage gap, gas gap and grain boundary segregation	Solid melt strengthening Reduces fatigue corrosion
C		Creates Cr <sub>23</sub> C <sub>6</sub>	Improves abrasion resistance Increases pourability

Titanium and titanium alloys have been used as biomaterials since 1930. Titanium has superior physical and chemical properties. Titanium is a lighter material than stainless steel and cobalt alloys (Titanium alloy 4.5 g/cm<sup>3</sup>, stainless steels 7.9 g / cm<sup>3</sup>, cast CoCrMo alloys 8.3 g/cm<sup>3</sup>, forged CoNiCrMo alloys 9.2 g/cm<sup>3</sup> specific gravity). The use of titanium as an inert material, non-toxic, light weight, good mechanical properties, easy production of small size samples, high biocompatibility, corrosion resistance, and proximity of the modulus of elasticity to

bone are widely used. Although titanium requires costly processing technology, it has many uses for aerospace, aircraft, medicine (hip and knee implants, heart valve, tooth filler, etc.), hand tools and even golf clubs due to the above-mentioned superior properties [5]. General mechanical properties of titanium and their alloys developed for orthopedic implants are given in Table 1.5.

Table 1.5: General mechanical properties of titanium and its alloys developed for orthopedic implants.

Alloy	Tensile Strength (MPa)	Pour Strength (MPa)	Elongation %	Elasticity Module (GPa)	Alloy Phases
ASTM grade 1	240	170	24	115	$\alpha$
ASTM grade 2	340	280	20	115	$\alpha$
ASTM grade 3	450	380	18	115	$\alpha$
ASTM grade 4	550	480	15	115	$\alpha$
Ti-6Al-4V	930	860	10-15	110	$\alpha + \beta$
Ti-6Al-7Nb	860	795	10	105	$\alpha + \beta$
Ti-5Al-2,5Fe	900	820	6	110	$\alpha + \beta$
Ti13Nb13Zr	970-1040	840-910	10-16	79-84	$\beta$
TMZF (Ti-12Mo-6Zr2Fe)	1060-1100	1000-1060	18-22	74-85	$\beta$
Ti15Mo	800	655	22	78	$\beta$
Ti-15Mo-5Zr-3Al	880-980	870-970	17-20	75-88	$\beta$
21 SRx (Ti-15Mo-2,8Nb-0,2Si-0,26O)	980-1000	950-990	16-18	83	$\beta$
Ti-(10-80)Nb	900-1030	760-930		65-93	$\beta$
Ti-16Nb-10Hf	850	730-740	10	81	$\beta$
Ti-Zr-Nb-Ta	650-1000		5-15	46-58	$\beta$
316L	500-1350	200-700	10-40	200	
Co- alloys	900-1800	500-1500	10-50	240	

### 1.1.2.2. Ceramic Biomaterials

Ceramic materials designed and manufactured for use in damaged, diseased and worn parts of the human body are called “bioceramics. The use of ceramics in the field of biomaterials is very wide. Bioceramics used in various shapes and different regions in the human body are used especially in dental prosthesis applications and orthopedic prostheses [4].



Bioceramics can be divided into three groups as bioinert, bioactive and biodegradable. In bioinert ceramics, fibrous tissue formation occurs at different thicknesses between the implant and tissue. This threadlike texture is produced to build a wall against the implant or to isolate the implant. Ceramics such as alumina and zirconia are examples of bioinert ceramics. In bioactive ceramics such as hydroxyapatite (HAP), bioactive glass, glass ceramics, bonding occurs at the interface between the implant and the tissue. This surface is called an active-bioactive surface. Biodegradable ceramics dissolve when the repair is complete in the body and are absorbed by the surrounding tissue and destroyed. For this reason, when using biomaterials of absorbable (resorbable) type, care should be taken to ensure that this material is chemically degradable and non-toxic by body fluids. Tricalcium phosphate (TCP) ceramics are biodegradable materials [4].

Contrary to the above properties, bioceramics have disadvantages such as being brittle, exhibiting low strength and low processing ability. Therefore, they should be used together with metallic biomaterials where mechanical properties are insufficient [11].

### **1.1.2.3. Polymeric Biomaterials**

The polymers are divided into two groups which are natural and artificial (synthetic) polymers. Starch, cellulose, natural rubber and DNA (genetic material) belong to the group of natural polymers. A large number of synthetic polymers are also available today. Examples of synthetic polymers are polyethylene (PE), polyurethane (PU), polytetrafluoroethylene (PTFE), polyacetal (PA), polymethylmethacrylate (PMMA), polyethylenteraphthalate (PET), silicone rubber (SR), polysulfone (PS), polyactic acid (PLA) and polyglycolic acid (PGA) [4].

The main characteristics of polymeric materials compared to metal or ceramic materials are that they provide ease of production in various ways (such as film, sheet, fiber,), low cost and ease of second processing. They are the most commonly used materials in places such as soft tissue and cartilage due to their flexibility [6]. However, for some applications; mechanical strengths are insufficient, they can swell by taking liquids into their structure or secrete unwanted toxic products in orthopedic area (such as monomers, antioxidants) [9].

#### 1.1.2.4. Composite Biomaterials

Composite is defined as the material formed by two or more materials having different chemical structures while preserving their properties. Thus, the composite material has the properties of two different materials that make up it. Composite material is obtained by the addition of various reinforcing materials into the material defined as “matrix. Various polymers can be used as matrix, and polymer fibers, glass, carbon, mica and powder ceramics can be used as reinforcing materials [4].

Composite materials are more advantageous compared to homogeneous materials. Because the properties of composite materials such as lightness, hardness, strength can be controlled by changing the material composition. When considered as biomaterials, the components that make up the composite material should be biocompatible. Examples of some composite applications in the field of biomaterials include: dental fillers, ultra-high molecular weight polyethylene (UHMWPE), orthopedic implants with porous surfaces [6].

### 1.2. HYDROXYAPATITE

The “Hydroxyapatite (HAP)” is most commonly used material as an alternative bone graft in surgical and biological activities which consists of calcium phosphate and anionic, cationic metal ions (For example:  $\text{Cl}^-$ ,  $\text{F}^-$ ,  $(\text{SiO}_4)^{-4}$ ,  $(\text{CO}_3)^{-2}$ ,  $\text{Mg}^{2+}$ ,  $\text{Na}^+$ ,  $\text{Al}^{3+}$ ,  $\text{K}^+$ ,  $\text{Zn}^{2+}$ , and  $\text{Sr}^{2+}$ , etc.) [18].

Hydroxyapatite (HAP) is the main component of bone and tooth and constitutes 60-70% of the total bone content [17-19]. Among the calcium phosphate components, HAP, the most stable phase in the pH range of 4.2-12.4, promotes bone ingrowth and does not cause toxicity, inflammation and foreign matter response [18,20].

Its excellent bioactivity and biocompatibility, as well as its capacity to increase cell adhesion and proliferation, enable HAP to be used in biomedical applications [21]. HAP is used for the correction of periodontal and bone defects, to produce bioactive coatings on dental pits, middle ear implants, tissue engineering, drug delivery systems, dental materials and on the surface of metallic implants [18].

Due to the chemical similarity of HAP to the mineralized bone of human tissue, synthetic HAP shows a high affinity to the host bone tissue and forms a chemical bond [22,23]. When the HAP-based ceramic material is placed in the body, a layer with no fibrous tissue and carbonated apatite forms on the surface of the material, contributing to the attachment of the implant to the living tissue, providing early implant stabilization and superior implant-peripheral tissue attachment [18].

Significant scientific developments related to HAP are given in Table 2.1 [24]. In 1952, the compared synthetic HAP with frozen bone to fill skeletal defects. The first X-ray diffraction studies on HA were performed in 1958 and the unit lattice dimensions were measured as  $a=b=0.943$  nm and  $c=0.688$ nm [23]. The commercialization of HAP-based bioceramics in dental and surgical applications took place in the 1980s [25]. Calcium phosphate-based coatings were also produced in the 1980s. In the following years, HAP powders of different morphology were produced and the structure of the HAP crystal was modified by various ion exchanges [24]. The important scientific developments related to HAP is given below Table 1.6 [24].

Table 1.6: Important scientific developments related to HAP.

Year	Invention
1965	Apatite precursor phase, Posner cluster
1969	Intensive HA synthesis for prosthetic applications
1975-1979	Clinical studies with TCP-TCP and HA
1972-1982	First commercial products (Ceros HA (1980), Durapatite (<1981), ProOsteon (1981), Calcitite (1982), Alveograph (1982))
1980-1987	Calcium phosphate coatings
1994	Production of HA whiskers by hydrothermal synthesis
1999	HA with Si ion exchange
2008	Pastry containing nano-apatite particles for bone replacement

The physical properties, compositions, chemical formulations, Ca / P molar ratios and solubility of HA and other calcium phosphate ceramics are listed in Table 1.7. HA with a Ca / P mole ratio of 1.67 is indicated by the chemical formula  $\text{Ca}_{10}(\text{PO}_4)_6(\text{OH})_2$  and has the lowest solubility compared to other calcium phosphates [26].

Table 1.7: Calcium phosphates and some properties.

CA/P ratio	Compound	Chemical Formula	Solubility at 25 °C $-\log(K_s)$
0,5	Monocalcium phosphate monohydrate (MCPM)	$\text{Ca}(\text{H}_2\text{PO}_4)_2 \cdot \text{H}_2\text{O}$	1,14
0,5	Monocalcium phosphate anhydride (MCPA or MCP)	$\text{Ca}(\text{H}_2\text{PO}_4)_2$	1,14
1,0	Dicalcium phosphate dihydrate (DCPD), bushite mineral	$\text{CaHPO}_4 \cdot 2\text{H}_2\text{O}$	6,59
1,0	Dicalcium phosphate anhydride (DCPA or DCP), monetite mineral	$\text{CaHPO}_4$	6,90
1,33	Octacalcium phosphate (OCP)	$\text{Ca}_8(\text{HPO}_4)_2(\text{PO}_4)_4 \cdot 5\text{H}_2\text{O}$	96,6
1,5	$\alpha$ -tricalcium phosphate ( $\alpha$ -TCP)	$\alpha\text{-Ca}_3(\text{PO}_4)_2$	25,5
1,5	$\beta$ -tricalcium phosphate ( $\beta$ -TCP)	$\beta\text{-Ca}_3(\text{PO}_4)_2$	28,9
1,2-2,2	Amorphous calcium phosphate (ACP)	$\text{Ca}_x\text{H}_y(\text{PO}_4)_z \cdot n\text{H}_2\text{O}$ , $n=3-4,5$ ; % 15-20 $\text{H}_2\text{O}$	-
1,5-1,67	Calcium-deficient hydroxyapatite (CDHA or Ca-def HA)	$\text{Ca}_{10-x}(\text{HPO}_4)_x(\text{PO}_4)_{6-x}(\text{OH})_{2-x}$ , $0 < x < 1$	~85
1,67	Hydroxyapatite (HA or HAP)	$\text{Ca}_{10}(\text{PO}_4)_6(\text{OH})_2$	116,8
1,67	Florapatite (FA veya FAp)	$\text{Ca}_{10}(\text{PO}_4)_6\text{F}_2$	120
1,67	Oxy Apatite (OA, OAp, or OXA), voelckerite mineral	$\text{Ca}_{10}(\text{PO}_4)_6\text{O}$	~69
2,0	Tetracalcium phosphate (TTCP, or TetCP), hilgenstockite	$\text{Ca}_4(\text{PO}_4)_2\text{O}$	38-44

HAP has a hexagonal crystal structure and can also be represented by the chemical formula  $\text{M}_{14}\text{M}_{26}(\text{PO}_4)_6(\text{OH})_2$ . M1 and M2 show two different crystal positions of 10 calcium atoms. The 4Ca atoms are in the M1 position and are surrounded by 9 oxygen atoms of the  $\text{PO}_4$  tetrahedra. The other 6 Ca atoms were coordinated with 6 oxygen atoms of  $\text{PO}_4$  tetrahedra and one of two hydroxyl groups [4]. The Ca (I) unit is located at the corners of the hexagonal lattice, the  $\text{PO}_4$  group near calcium is capable of bonding with live bone tissue. The atoms in the Ca (II)

position form an equilateral triangle with the structural hydroxyl group column in the middle [27]. HAP crystal is shown schematically in Figure 1.2 [28,29].

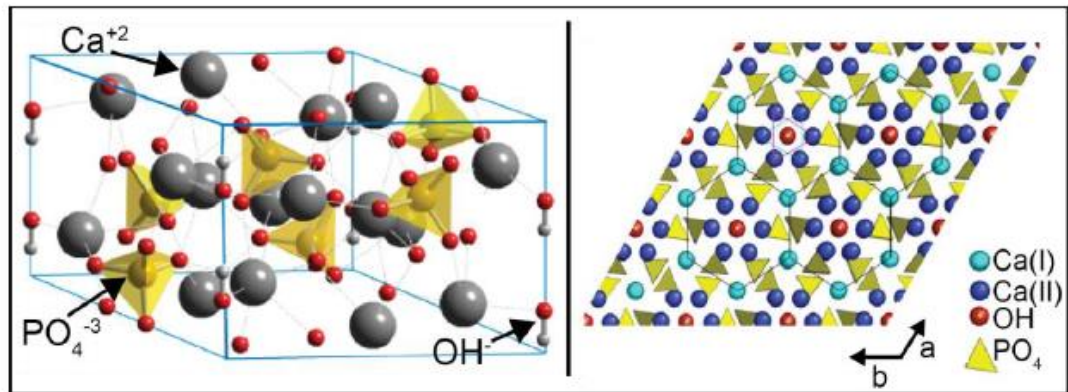


Figure 1.2: Dimensional HAP crystal and HAP structure along the c-axis.

Figure 1.3 shows the solubility diagrams of calcium phosphate components [30,31]. TTCP and DCPD are two calcium phosphate minerals with the highest solubility at pH above and below 7.6. HAP is the most stable phase in a wide pH range (where the pH is greater than  $\sim 4$ ) [30].

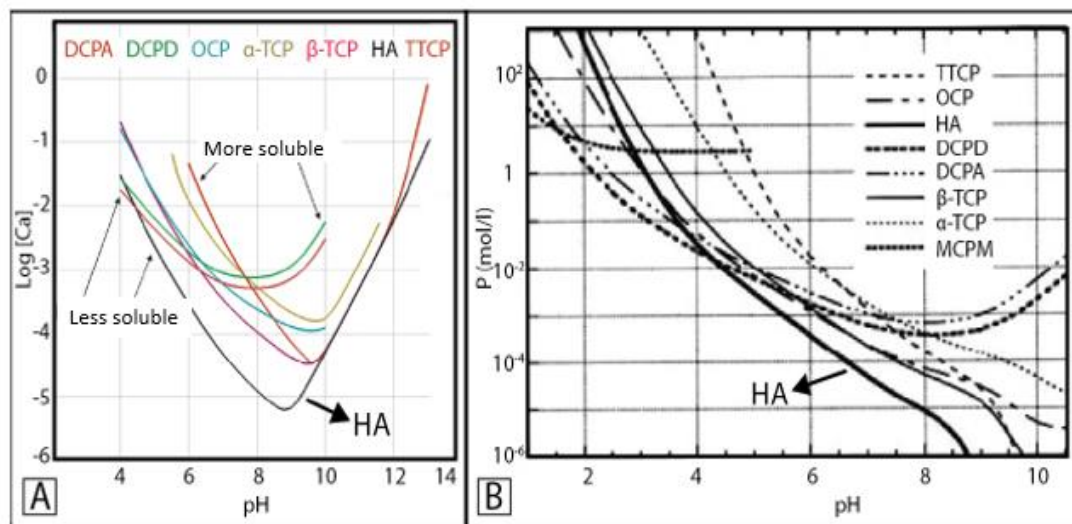


Figure 1.3: Solubility of calcium phosphate species according to a) calcium and b) phosphate concentrations.

### 1.3. SOL-GEL

This method is formed by shortening the words solution and gelling as sol-gel; liquid and colloidal solid particles to form a stable suspension “left”, precipitation of colloidal particles containing abundant water-type precipitate-type structure consists of “gel” steps. Sol-gel process can be defined as the process of synthesizing gel from alkoxides. In another definition, the sol-gel process is defined as the final product of the solution or suspension desired to be obtained by removing the solvent from the system after gel formation is achieved by colloidal particles agglomeration [32-34]. The most general definition is sol-gel treatment; colloidal formation of inorganic webs (gels) by means of suspensions (sol) and subsequent formation of the web structure in solid phase [36].

The residuals can be defined as the suspension of small colloidal particles in which the effect of gravitational forces are ignored and forces such as Van der Waals forces and surface loads are effective. [34] The solid particles in the sol should be denser than the solvent liquid. Generally, the size of the colloidal residual particles varies between 2 nm and 0.2  $\mu\text{m}$ . If the colloidal particles are found in the gas, the resulting structure is called aerosol [32-35]. The gel is formed by overfilling the porous reticulated structure. This conversion requires hydrolysis and condensation reactions [36]. The overview of sol-gel process is shown at Fig.1.4 [37].

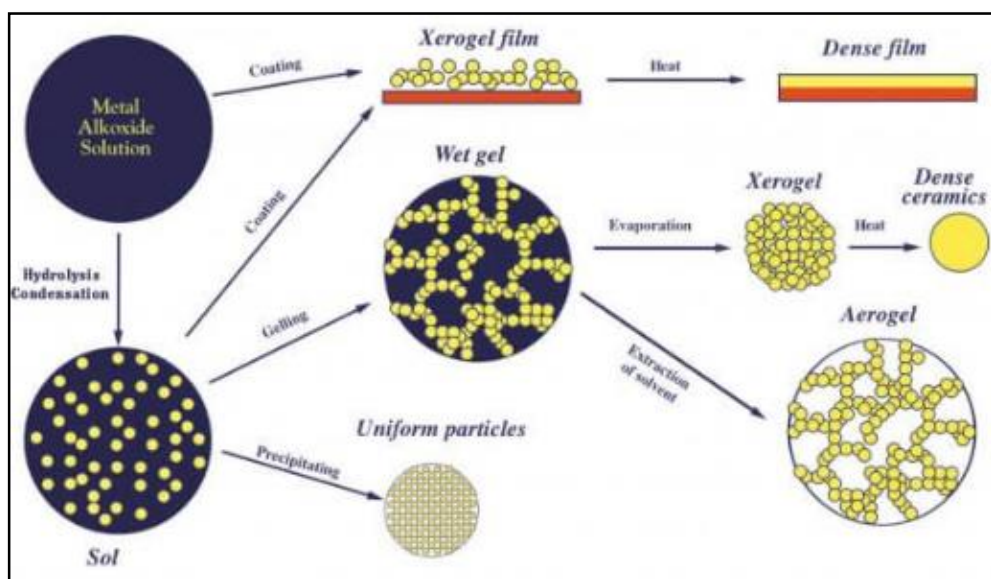


Figure 1.4: Sol-gel process.

The steps of the sol-gel treatment are simply summarized:

- Preparation of homogeneous solution with molecular precursor
- Solvent solution from homogenous precursor solution as a result of hydrolysis reaction
- As a result of the condensation reaction, the suspension of the left suspension changes to a gel state.
- Shaping the gel
- Processing the formed gel to obtain the targeted product

In 1846, the first work on the sol-gel treatment was carried out by J. Ebelman, and the reaction of tetraethoxysilane with moisture produced silicate monoliths. However, intensive studies on sol-gel began in the 1930s; industrial applications were observed in the 1950s. Today, coated fibers; This method is used in various fields such as insulating materials, inorganic hybrid materials, glasses and fillers. [35,38,39].

The advantages of the sol gel method can be listed as follows:

- Can work in atmospheric environment.
- Can be used at low reaction temperatures. In this way, solution losses caused by evaporation can be minimized, interactions with reaction vessels are prevented; thus high purity is achieved, air pollution is reduced and energy can be saved.
- We can carry out reactions in small reaction vessels; large and complex systems are not required.
- Since it is working at low temperatures, it allows easily inorganic, organic or biological molecules to be doped into inorganic networks.
- Crystal and amorphous products can be obtained.
- High purity end product can be obtained.
- Since the process is in solution environment, it has easy controllable parameters. Thus, products with controlled pore size and distribution are obtained.
- Can be used for micro or nano-sized materials.

- The material obtained is resistant to heat, chemical, light and microbial damages [32,36,40].

In addition to its advantages, there are disadvantages of the sol-gel process. These include;

- Relative cost of raw material,
- Long process time,
- Difficulties in keeping the solution at constant viscosity during the gelling step,
- Difficulties in converting wet gel to dry gel due to stress differences caused by removal of solvent from the system,
- Solvents used are harmful to health [53,57,61].

### **1.3.1. Steps of Sol-Gel**

In the sol-gel process, metallic salts and alkoxides are used as starting materials. The solvent chemistry to be used for the two groups used as the precursor is very different from each other. Generally, water or organic solvent is preferred as the solvent. The precursors contain a metal, surrounded by various ligands form the residue [34]. A ligand is an ion or molecules that can be attached to the central metal atom to form a complex. In particular, alkoxy structures and metal alkoxides are used extensively.

Metal alkoxides are members of the family of metal organic compounds. Alkoxides are organic ligands which combine with metal or metalloid atoms [43].

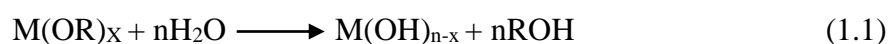
Metal alkoxides of general formula  $M(OR)_n$  are compounds formed by the coupling of the alkoxy group of the metal cation formed by removal of a hydrogen from the hydroxyl group of the alcohol. In another definition, metal alkoxides are referred to as organic ligands capable of forming compounds with metal or metalloid atoms. Most used metal oxides include tetramethoxysilane (TMOS) and tetraethoxysilane (TEOS) [36].

The sol-gel treatment is essentially based on two reactions. These two reactions are hydrolysis and condensation reactions [32, 36, 42].



### 1.3.1.1. Hydrolysis reaction

The reaction of the metal atom by the addition of hydroxyl ions is called the hydrolysis reaction. The hydrolysis reaction of alkoxides is a nucleophilic displacement reaction. When nucleophilic molecules such as water react with alkoxides, a rapid exothermic reaction occurs. In the hydrolysis reaction, the nucleophilic water molecule transfers a proton to the alkoxide group. Thus, by replacing hydroxyl groups (-OH), oxo (-O-) and alkoxy groups (-OR). The reaction in Eq 1.1 takes place [43].

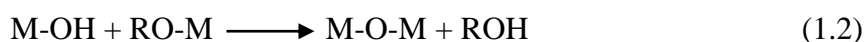


Alcohol is produced as a by-product in this reaction. Depending on the amount of water and catalyst, all OR groups in the hydrolysis reaction can be replaced with (-OH) groups or the hydrolysis can be completed [41].

We obtain medium and low cross-linked metal particles by hydrolysis products in solution. The resulting sol are suspensions which are stable, transparent and containing particles having a particle diameter of less than 50 nm. The prepared nanosols have high storage stability, fast drying times even at low temperatures and good adhesion to many material, since they contain alcohols of hydrolysed precursors. Thanks to the alcohol they contain, fibers swell and reduce surface tension; this facilitates the wetting of the surface and ensures better film formation. Cracks are reduced; The fibers are coated [44-48].

### 1.3.1.2. Condensation reaction

Two metal alkoxides are formed by the condensation reaction of the metal oxides formed by hydrolysis. The condensation reaction may begin before the hydrolysis reaction is finished; therefore, these two reactions cannot be separated clearly [49].



Eq 1.2. Condensation reaction with alcohol as a by-product (olation reaction) [32,36].

Olation is the condensation process that forms the hydroxy bridge between two metal-centered molecules and the alcohol group emerges as a by-product [32, 36].



Eq.1.3. Condensation reaction which gives water as a by-product (oxalation reaction) [32,36].

Oxidation is the condensation process that forms a –O- bridge between two metal-centered molecules and water (H<sub>2</sub>O) emerges as a by-product [32, 36].

Rates of these two reactions:

- Hydrolysis environment,
- The alkyl group in metal alkoxide,
- Solution pH and concentration,
- Reaction time and temperature,
- Catalysis concentration,
- It depends on the molar ratio of water with alkoxide ( $R = [\text{H}_2\text{O}] / [\text{alkoxide}]$ ) [32, 36, 44, 45].

### 1.3.1.3. Polymerization

With the selection of suitable catalysts, as condensation reactions grow, they are polymerized by bonding together in large bundles. The polymerization may continue through olation or oxidation. When the solution starts to be mixed, polymerization (polycondensation) and hydrolysis reactions occur in too many sites [50,51].

In acidic medium weakly branched dense microporous polymeric reticulate structures, in the basic medium high-branched small porous colloidal structures are obtained [51].

#### **1.3.1.4. Gelation**

Polymerization reaction of metalloxanes formed by condensation reactions results in structures of different sizes. These structures expand and intertwine throughout the solution to form a reticulated structure called gel. The polymeric gels are covalently bonded. In granular gels, Van der Waals forces prevail. Depending on the rate of formation of the reaction, the microstructure of the gels can be controlled. In systems where only alkoxides are used, a system which cannot be recycled is formed as a result of the enamelling of the polymers formed by the addition of water. By heating the gel in particulate suspensions, solids can be obtained by removing the solvent molecules and water present in the pores, making the system supersaturated, and returning to the system [41].

#### **1.3.1.5. Aging**

After the gelling step, bond formation continues. The bonding between small particles and polymers continues as the gel is still left in the network. The aging step is the process of changing the structure and characteristics after the gelling process. As the solvent is removed and the interaction between the particles causes the network to contract. This is called shrinkage [41].

#### **1.3.1.6. Drying**

If evaporative drying is carried out under normal atmospheric conditions, the jelly web will contract due to capillary pressure. This drying gel is called xerogel. If the wet gel is placed in an autoclave and dried under supercritical conditions, no interface is formed between the liquid and the solid; no capillary pressure. Shrinkage occurs very little. The resulting product is called aerogel [41].

#### **1.3.1.7. Coating**

Coating methods of the sol-gel method:

- Immersion method

- Spraying method
- Spin method
- Drainage method
- Printing method [41].

The thickness of the coating is determined by viscosity, solids content, drying rate, surface tension and coating speed. The structure of the coating depends on the composition of the sol. The higher the capillary pressure and the smaller the size of the pores, weaker the condensation. The structure of the dried coating is dependent on the capillary force pressure and the intensity of the condensation reaction. The bonds are broken due to the breakage of over-shrinking structures' coating quality [51-57]. In Fig.1.5. a) dip coating and b) spin coating metods can be seen.

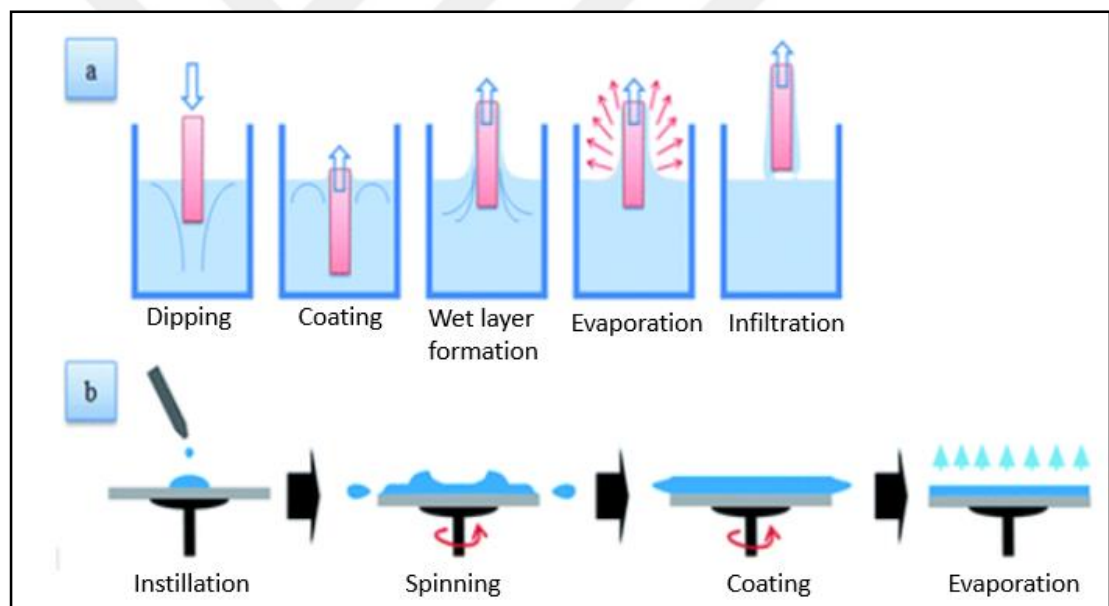


Figure 1.5: Some of the coating methods used in the sol-gel method, a) Dip coating, b) Spin coating.

### 1.3.2. Sol-gel Coating of Materials

Hydrolysis, condensation and drying conditions affect the porosity, mechanical properties, coating thickness and density of the coating in the coating of materials. The heat treatment provides good adhesion of the coated surface to the material and provides a more durable coating. By adjusting the annealing temperature and time,

the physical and mechanical properties of the material can be improved. However, since the decomposition temperatures of materials are low, annealing is not performed at very high temperatures [59-60].

It is possible to add different features to materials by improving the physical and chemical properties using sol-gel method. Chemical modification is covalently bonded to the metal oxide matrix of the additives. The chemical modification can also be formed by bonding different metal alkoxides to each other or by using the (-R) group of the organic side component.

In the physical modification, additives such as pigments [63], oxides [64], organic polymers [64-67], dyes [68-70], inorganic colloidal metals [71-74] and biomolecules [74-81] are added to the prepared nanosol. The solution is made by preparing or joining after the hydrolysis reaction.

The ability to combine physical and chemical modifications and make them easy to apply to the sol-gel coating provides unlimited functionality and development of materials with limitless application and development potential. Functionalities of materials by sol-gel method is shown at below Fig.1.7.

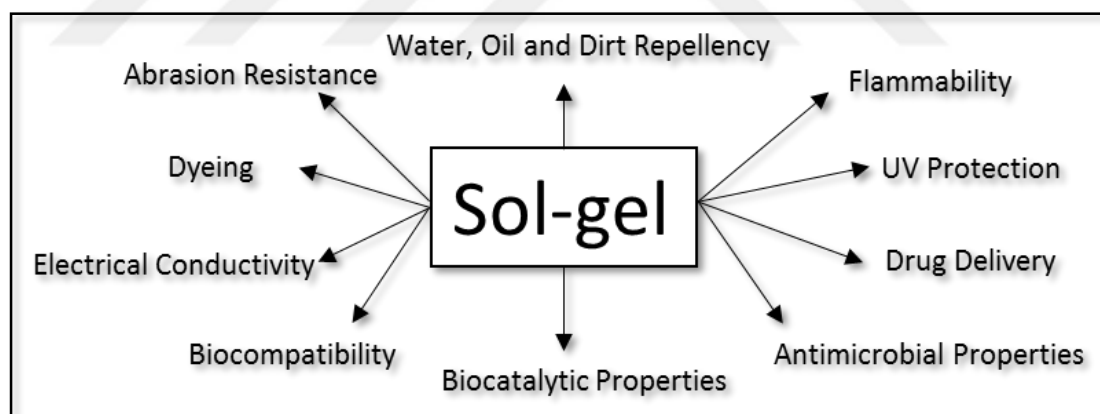


Figure 1.6: Functionalities of materials by sol-gel method.

With nanosol coatings, metal oxide based particles smaller than 50 nm in diameter show very good adhesion properties on textile materials. The layers obtained are resistant to chemical, biological, heat and light effects. Besides functionalities, these coatings add strength and abrasion resistance to materials. Sol-gel nanosol coatings are applied to materials with impregnation and exhaustion

methods in finishing processes at room temperature and normal atmospheric pressure [58].

### 1.3.3. Dip Coating

Dip coating is one of sol-gel's process which substrates immerse and lift up from the liquid under controlled atmosphere and temperature. This substrate should be smooth and immerse-lift-up movement should be vibrationless. To achieve a better coating quality, the dipping speed, minimum vibration and smooth surface are required. The thickness of the coating depends on layers thickness, viscosity of fluid and lift-up speed [82,83].

Dip coating steps:

- Immerse
- Lift up
- Coating
- Infiltration
- Evaporation

The frontier layer occurs on the coating surface when the substrate immerses. This frontier layer divides the coating into inner and outer layers during coating and infiltration steps. Inner layer moves in the same direction with sublayer and outer layer moves in opposite direction.

Dip-coating process's forces are:

- Substrate lift up force because of viscosity
- Surface tension
- Gravity
- Inertial force of frontier layer
- Surface tension gradient
- Fracture pressure [84].

## 1.4. Properties of Zinc Oxide

Zinc oxide which crystallizes in hexagonal structure is indicated as “ZnO” and is found as “mineral zinkite” in nature. The lattice constants of ZnO, shown in the crystal structure in Figure 1.8, are  $a = 3,24982 \text{ \AA}$  and  $c = 5,20661 \text{ \AA}$ . This structure is called z hexagonal wurtzite. The compound ZnO is a semiconductor of the group II-IV [85].

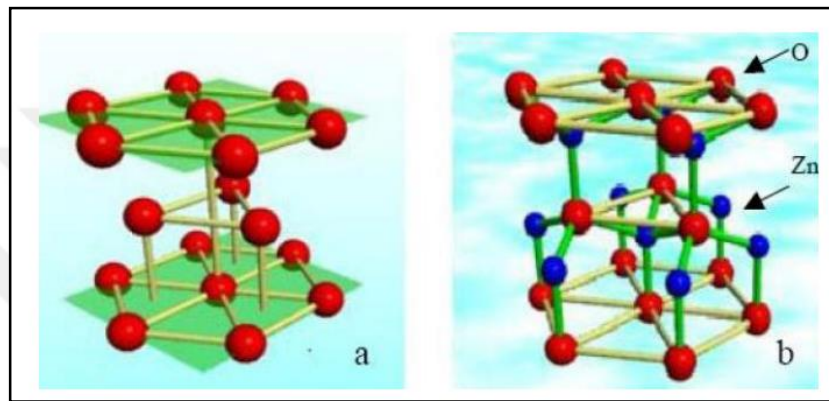


Figure 1.7: a) Hexagonal wurtzite structure b) ZnO crystal structure.

ZnO has a high electrical conductivity and has a wide range of applications in optical and electrical fields. The cost of zinc oxide coated thin films is low due to the abundance of zinc in nature. ZnO has 80-90% optical permeability in the visible region. Due to ZnO films' transparency is in visible light; the produced films draw attention as transparent conductive materials. It also has electrical resistance between  $10^{-1}$ – $10^{-4} \Omega\text{cm}$ . ZnO reacts with organic and inorganic acids. In addition, zinc oxide dissolves in ammonia solution to form zinc acetate. ZnO is white and turns yellow at  $300^\circ\text{C}$  [86].

Besides being an inorganic antimicrobial material, ZnO provides superior properties to the material with its functionality such as electrical conductivity, photocatalytic and anti-reflective features and UV absorbability. Non-toxicity ensures safe use. ZnO is applied to textile materials by various methods. ZnO application with antimicrobial bandages. [87-92]. The fundamentals of ZnO in  $300^\circ\text{K}$  is shown in below Table 1.8.

Table 1.8: Some of the properties of ZnO at 300 K.

Properties	Value
a	0.32495 nm
c	0.52069 nm
a/c	1.602 (normal value for hexagonal structure 1.633)
Density	5.606 g/cm <sup>3</sup>
Melting Point	1975 ° C
Thermal Conductivity	0.6-1.2 W/cm-K
Static dielectric constant	8.656
Refractive index	2.37
Energy band interval	3.3 eV
Resistivity	10 <sup>-1</sup> - 10 <sup>+4</sup> Ω cm
Crystal Structure	Wurtzite

Zinc oxide has superior performance in reflecting the incoming light and has anti-reflective properties due to its roughness on the surface and absorbability of light. For this reason, anti-reflective coatings with ZnO are used in versatile applications such as glasses, glass showcases and building glasses with sol-gel method [54,67].

The antibacterial mechanism of zinc oxide is explained in the literature by active oxygen structures. [93] Swai (2003) in his study shows that, ZnO particles at atmospheric conditions, in moist media (hydrogen peroxide - H<sub>2</sub>O<sub>2</sub>) causes the formation of active oxygen. H<sub>2</sub>O<sub>2</sub> affects and damages the membranes of bacteria cells. Thus, they inhibit the growth of bacteria or cause the death of bacteria. On the other hand, superoxide anions (O<sub>2</sub><sup>-</sup>) oxidize bacteria cells very strongly due to the presence of active radical oxygen [94-96].

ZnO particles have a detoxifying feature. Rajagopalan et al. (2002) tried to explain this mechanism and used paraoxone toxin. ZnO particles are the destructive absorption mechanism that catalyzes paraoxone, thereby breaking the P-O bond in the paraoxone toxin [97].

After coating the surface with ZnO sol-gel method, hydrothermal method is used to enlarge the nanorods [98].

ZnO nanoparticles are trapped in the polymer matrix as a result of the electro forces. In studies, particles lose their UV protection when trapped in the polymer



matrix. Therefore, if it is desired to gain UV protection, coating should be done on the medium [98-99].

## **1.5. Properties of Iron**

In 2001 the first in vivo test was conducted to demonstrate the biosafety of pure iron. After that test, iron-based materials have been confirmed as a promising candidate for biodegradable applications. During the years, pure iron has become one of the most widely researched biodegradable materials [100]. Iron (Fe) is represented as traditional engineering material which has plenty of advantageous such as excellent mechanical properties, superior machinability, and accessible price. The fundamental advantages of Fe-based materials make them potentially exceptional source of biodegradable metallic materials for the medical field [98]. Based on previous studies, iron applications in medical field consist of three main categories: intravascular stents, implant materials for bone surgery and scaffolds for bone tissue engineering.

The Fe-based materials are significant because of their excellent mechanical properties and biocompatibility as one of the main types of biodegradable metallic materials. The previously conducted researches already showed that the Fe-based biomedical materials can be successfully produced by many techniques. The biocompatibility studies, both in vitro and in vivo, together with mechanical researches, proved that the Fe-based materials are potentially useful for applications in bone tissue engineering [102].

There are two important parameters regarding to these materials: degradation rate and corrosion mode. The degradation rate can affect biocompatibility of the material. When the degradation rate yields got lower, the biocompatibility gets better. Corrosion mode as the second parameter is quite important issue which directly in relation with safety and implant efficacy. The ideal corrosion mode is uniform corrosion [103].

Based on the information above and previous studies, it can be said that the biodegradable Fe-based materials are quite promising and have positive effects on bone tissue engineering.

## **1.6. Relation between Bacteria - Implant and Infection**

Surgical procedures which use implants are often faced with two problems. First, the tissue mismatch between the implant and the host, and the other is biomaterial-centered infections [104]. So far, successful tissue integration; It is possible by attaching the biomaterial to the host tissue. During bonding, chemical bonds are established between the surface of the biomaterial and the host cell [105]. A race begins between bacteria and tissue cells to attach to the surface of the biomaterial. This race determines the formation of the implant surface. If the tissue cells first settle on the implant surface, the implant is protected. In this case, the biomaterial surface is protected from bacterial colonization. Otherwise, bacterial colonization will occur on the surface of the implant and the infection process will begin [104].

Studies in the natural ecosystem have shown that more than 99.9% of the bacteria are immobilized on the inland surfaces, forming micro-biofilms and living in these biofilm layers [106]. These bacteria, which colonize on biomaterials, also adhere to biomaterials and grow in biofilm layers [107]. The implant material placed on the femoral bone of a patient was examined after removal and it was observed that there were bacterial colonies in biofilms covered with glycocalyx (a layer of carbohydrate bound to membrane protein and lipids on the outer surface of cell membranes) [108].

The ability to adhere to a surface is found in almost all bacteria, and its colonization depends on the surface of the biomaterial, the surrounding liquid area and the characteristics of the bacteria [104]. Once the biomaterials are placed in the host tissue, glycoprotein biofilms containing fibrinogen, fibronectin, collagen and other proteins are formed. These biofilms cover the contact surfaces of the biomaterial and host tissue. Thus, the receptor region is formed where host tissue cells and bacteria are attached [109, 110]. The macromolecular structure of this film has a particular role for each organism or tissue cell. In studies conducted on the formation of biofilm layers in materials such as ceramic, glass and titanium, it has been observed that osteointegration is prevented by biofilm layers [110].

Today, most of the biomaterials used in orthopedic surgery consist of metals and polymers. Biomaterials in the biological environment, dead tissues and foreign bodies are passive in the biological environment after they are placed in the body and are physically chemically active and also have low resistance to infections [111].



## 2. EXPERIMENTAL

### 2.1. General Overview of Zn-Fe doped HAP Process

The general overview of Zn-Fe doped HAP process was shown at below flow chart as Fig 2.1.

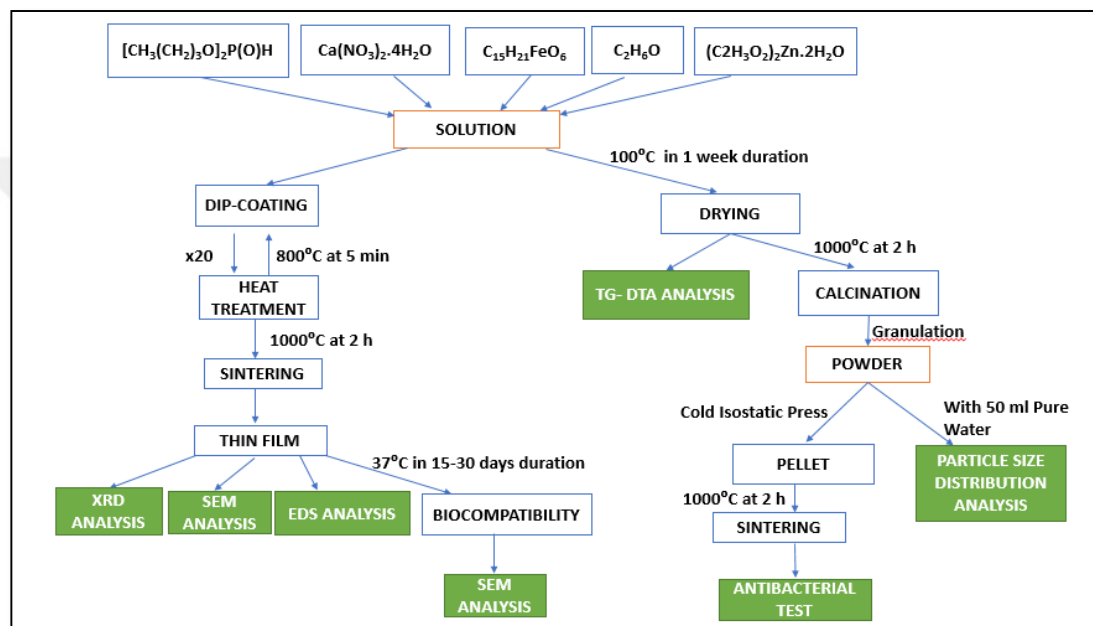


Figure 2.1: General overview of Zn-Fe doped HAP process.

### 2.2. Preparation of Silicon Wafers

Cleaning of silicon wafers is important for thin film to be able to grip the surface homogeneously. Uncleaned substrates may prevent the film from forming in a homogenous manner and may negatively affect the accuracy of the measurements.

Silicon wafer substrates were cut to the desired size with a diamond tip cutter and were initially left overnight in hydrochloric acid (HCl). After they were cleaned in pure water and ethanol in ultrasonic titration bath for 3 minutes, they were dried with a heat gun. Afterwards the wafers were kept at 100°C for one hour in furnace. Subsequently, thin film coating process was started and thin film coatings were

carried out at room temperature. The steps of the cleaning process were shown in Figure 2.1.

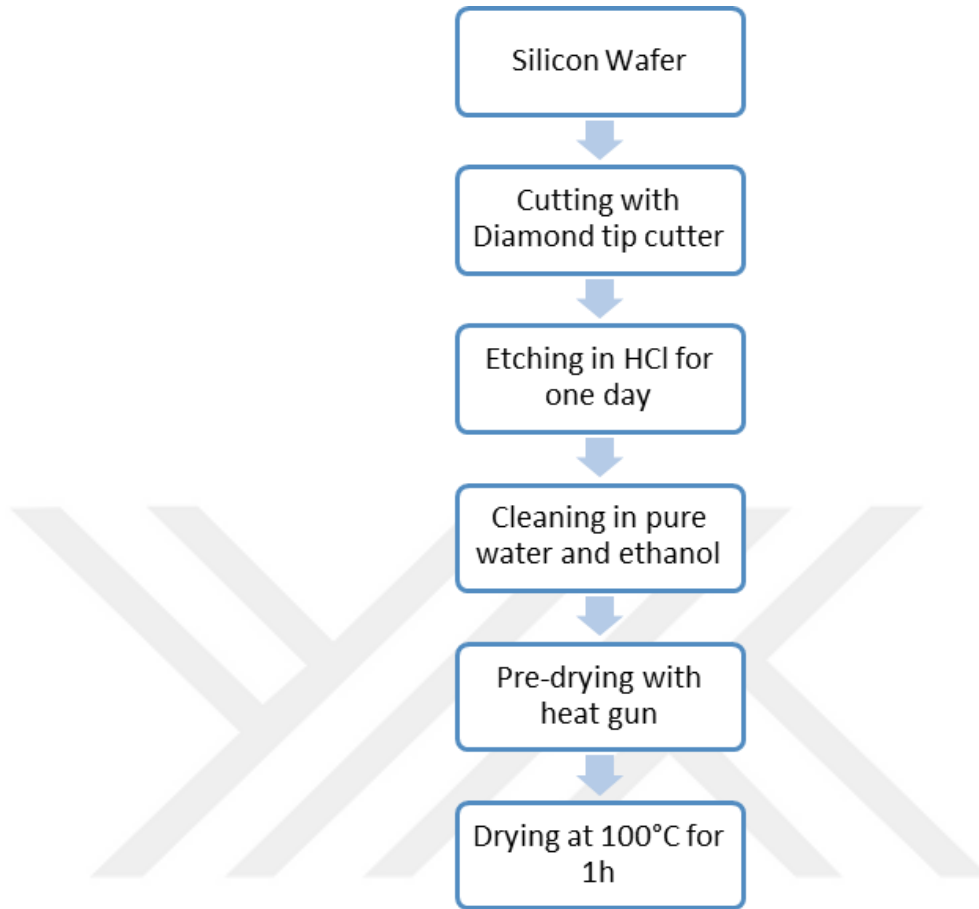


Figure 2.2: Silicon Wafer (100) Cleaning.

### 2.3. Preparation of Sol-Gel, Thin Film and Heat Treatments

Before the preparation of the solution the beakers were cleaned with pure water, ethanol ( $C_2H_6O$ ) and pure water relatively in ultrasonic titration bath for 3 minutes. After that the beakers were dried with heat gun until there was no residue seen during visual control. Those beakers were put in furnace for 1h at 100°C and left to be cooled to room temperature.

First step of solution preparation was to make Hydroxyapatite (HAP) solution. Then the doping materials were added into that solution. The used chemicals for HAP solution was given in below, Table 2.2.

Table 2.1: The formulae of HAP Precursors.

Chemical	Formula	Mole (g/mole)	Trademark and Purity (%)
Dibutyl Phosphate (DP)	[CH <sub>3</sub> (CH <sub>2</sub> ) <sub>3</sub> O] <sub>2</sub> P(O)H]	194,21	Aldrich %96
Calcium Nitrate Tetrahydrate (CNT)	[Ca(NO <sub>3</sub> ) <sub>2</sub> .4H <sub>2</sub> O]	236,15	Merck %99
Ethanol	[C <sub>2</sub> H <sub>6</sub> O]	46	Merck %98

The created HAP solutions were separated to different amounts of doping criteria. The doped iron and zinc formula was shown in Table 2.3. The total used amounts of Zinc/Iron co-doped HAP solution was mentioned in below, Table 2.4.

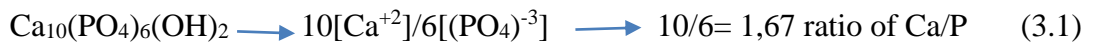
Table 2.2: Iron and Zinc Formula.

Chemical	Formula	Mole (g or mole)	Trademark and Purity (%)
Zinc Acetate Dihydrate (ZAD)	[(C <sub>2</sub> H <sub>3</sub> O <sub>2</sub> ) <sub>2</sub> Zn.2H <sub>2</sub> O]	219,5	Aldrich %98
Iron(III) Acetylacetonate(I(III)A)	[C <sub>15</sub> H <sub>21</sub> FeO <sub>6</sub> ]	353,1 8	Merck %99

Table 2.3: The total used amounts of Zinc/Iron co-doped HAP solution.

Sample	DP(g)	CNT(g)	ZAD(g)	I(III)A(g)	Ethyl Alcohol
1 (0,0005 mole Zn-Fe DOPED)	2,320 g	4,484 g	0,109 g	0,176 g	50 ml
2 (0,0010 mole Zn-Fe DOPED)	2,320 g	4,248 g	0,219 g	0,353 g	50 ml
3 (0,0015 mole Zn-Fe DOPED)	2,320 g	4,012 g	0,328 g	0,529 g	50 ml
4 (0,0020 mole Zn-Fe DOPED)	2,320 g	3,776 g	0,438 g	0,706 g	50 ml
5 (0,0025 mole Zn-Fe DOPED)	2,320 g	3,540 g	0,547 g	0,882 g	50 ml
6 (0,0030 mole Zn-Fe DOPED)	2,320 g	3,304 g	0,657 g	1,059 g	50 ml

The solution was oriented according to solution preparation flow chart shown at below steps in Fig.2.2. Each sample's molarity has been calculated by using molar ratio in HA formula molar Equation 3.1.



To stabilize the molar ratio of Ca/P, after doping the CNT amount has been re-calculated and decreased according to the increased amount of doped iron and zinc. (Eq. 1) The solutions were mixed on magnetic mixer device with the speed rate of 200rpm for 1h in order to achieve homogeneous, non-sagged/agglomerated solutions which are named as sol-gel solutions. After the mixing step each solution has been controlled visually.



Figure 2.3: Preparation of the Solution.

Prepared sol-gel solutions were coated on silicon wafers (100) by using KSV Dip-Coater device. The wafers were immersed (coated) in the sol-gel solution at a rate of 100 mm / min. The coating steps were repeated 20 times. After each coating, the samples were heated to 800°C for 5 minutes in furnace to remove the organics from the surface. The final heat treatment was done after 20 times of coating at 1000°C for 2 h and left in the furnace to cool down for one night. After the heat treatment the thin film samples were checked visually. The flow chart of dip-coating steps until thin film formation was shown in Fig.2.3.

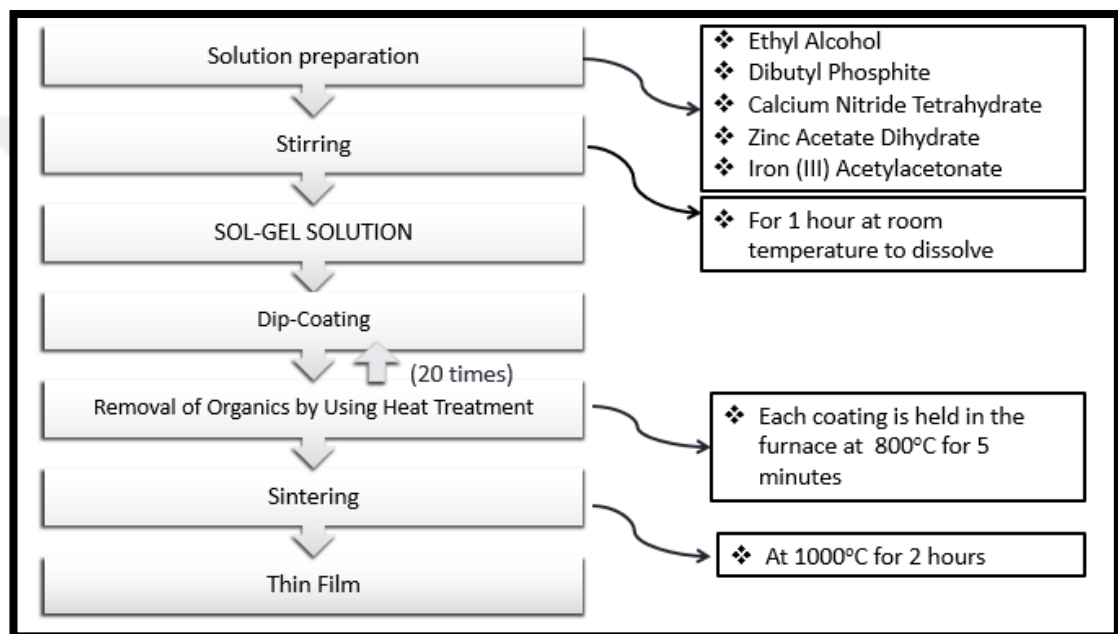


Figure 2.4: Flow Chart of Thin Film Formation in Dip-Coating.

## 2.4. Preparation of Simulated Body Fluid (SBF)

Firstly, after cleaning steps of beakers, 700 ml pure water had been heated up to body temperature, which is 37°C. Secondly, the chemicals which were shown in Table 4 was added respectively to the pure water. The addition was made after each chemical has been dissolved in the solution. To prevent dissolution and turbidity 0,083 M HCl (Hydrochloric acid) was added; 15 ml and 25 ml respectively in the solution. After that 300 ml pure water was added and the chemicals were stirred in magnetic mixer to obtain required transparency of the solution. The pH value was



measured as 7,5. This solution preparation method was based on Kokubo SBF model.

The prepared thin films were put into the simulated body fluid solution for 15 and 30 days separately. However, after every 2 days the SBF solution was changed, because SBF dissolves to  $\text{Ca}^{+2}$  and  $\text{P}^{+3}$  ions in the solution which may cause the complete thin films solvation. After 15 and 30 days the films were observed in SEM (Scanning Electron Microscope) in order to analyze the microstructure of the films. The chemical steps of SBF preparation was shown at Fig.2.5.



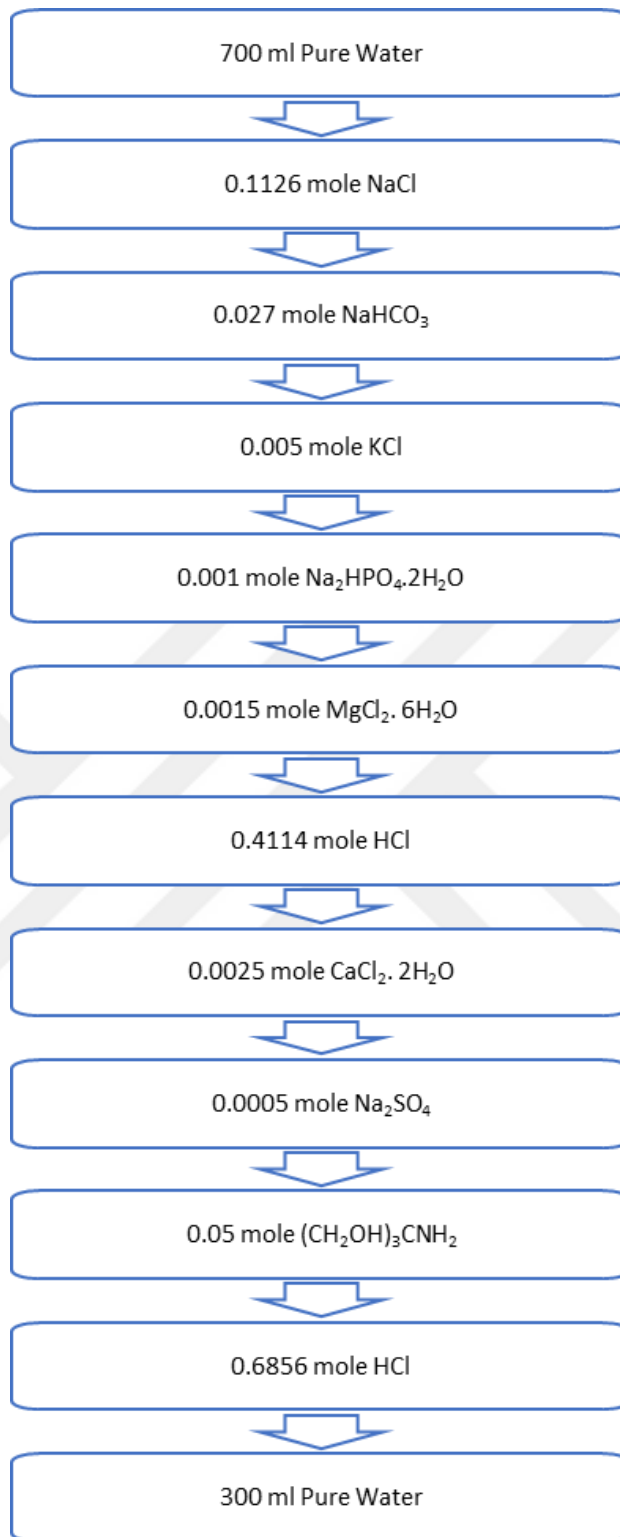


Figure 2.5: Chemical steps, formulae and the mole of SBF.

## 2.5. Preparation of Zn-Fe co-doped HAP Powder for Particle Size Distribution and Preparation of Antibacterial Test

### 2.5.1. Particle Size Distribution

The solutions containing in various amounts Zn-Fe doped HAP were prepared as mentioned in... and dried in furnace for 1 week at 100°C. The dried bulk samples were sintered in the furnace for 1h at 1000°C. After that the sintered specimens have been grinded as 5µm to be able to have homogeneous distribution. Then 3g of grinded powders were dissolved in 30ml pure water and analyzed in particle size distribution device Mastersizer 2000.

The flow chart of this analysis was shown at below Fig.2.5.

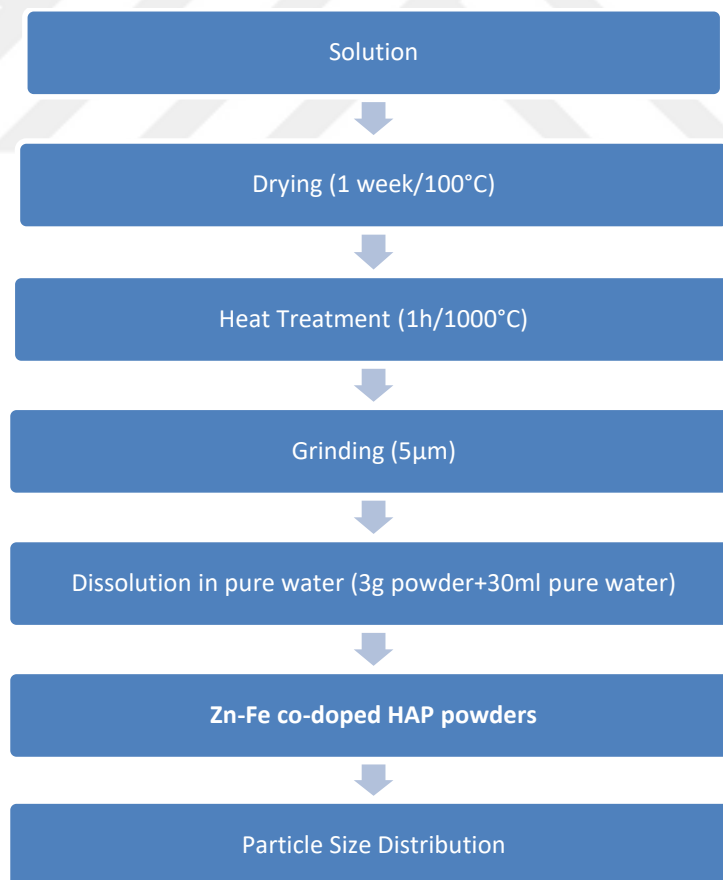


Figure 2.6: Preparation of particle size distribution analysis.

### **2.5.2. Preparation of Antibacterial Test**

The Zn-Fe co-doped HAP powders were put in cold isostatic press to be shaped as pellets. And these pellets were sintered in the furnace for 2 h at 1000°C.

For the bacterial test medium *Staphylococcus Aureus* bacteria were used as infection-caused-bacteria. They were put in Petri dish, where Mueller Hinton broth contains, and left for 24h in centrifugal system at body temperature. After the bacteria reaches the maximum growth, the pellets were put in Petri dish and left the medium for 1 week in order to see the antibacterial functionalities.

### **2.6. Chemical Composition, Phase Analysis and Microstructure of Thin Films**

The samples were analyzed in D8 ADVANCE Bruker X-ray Diffraction device (XRD) at a range of 28-42° with 0,1 degree/ min speed under Cu-K $\alpha$  (wavelength 0,154 nm) radiation ambient. SEM was used to determine the grain distribution, the presence of porosity, orientations of the grains, crack and secondary phases. Before the SEM analysis, thin films were coated with gold for 40 seconds to be conductive.

EDS is a device which is connected to the SEM. In EDS analysis the distribution map of the elements and the distribution of the elements (Ca, P, O, Fe, Zn) in thin films were investigated.

## 3. RESULTS

### 3.1. Partical Size Distribution

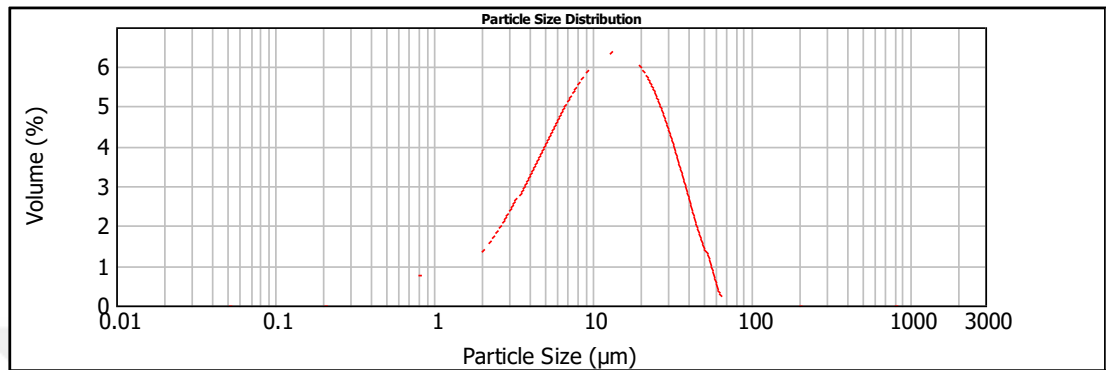


Figure 3.1: Particle Size Distribution.

Fig. 3.1 represents grain size distribution analysis of %0.0001 M doped HAP powder. Particle sizes are approximately between 1-100 micrometer according to the analysis.

In this study, antibacterial properties of pellets obtained with / without HA powders were investigated. Since no particle size reduction or homogenization studies have been carried out, particle size has varied in nm and µm scale.

### 3.2. TG/DTA Analysis

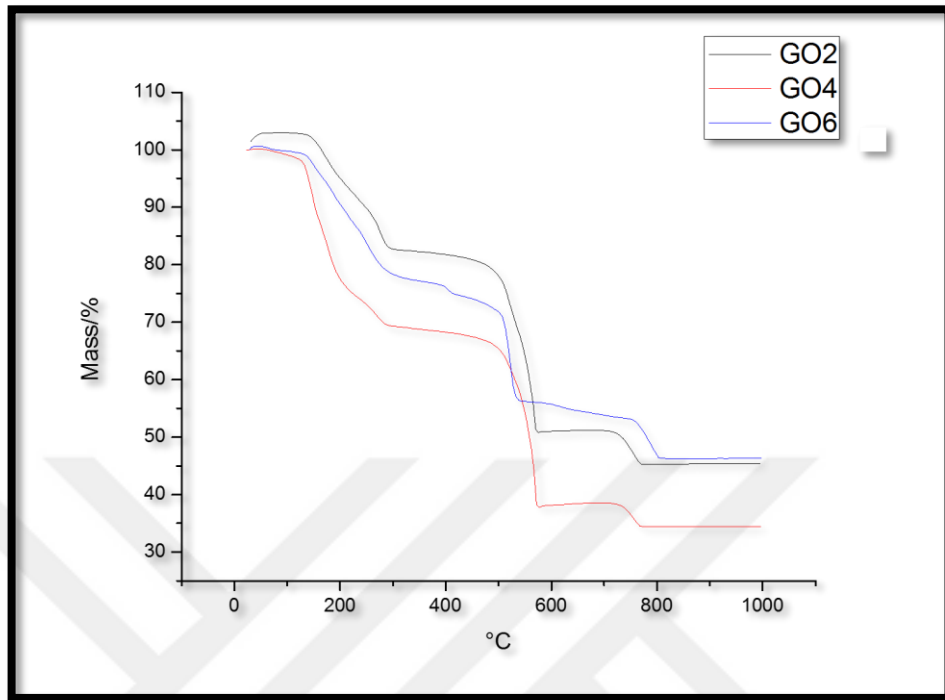


Figure 3.2: TG Analysis of Zn-Fe co-doped HAP.

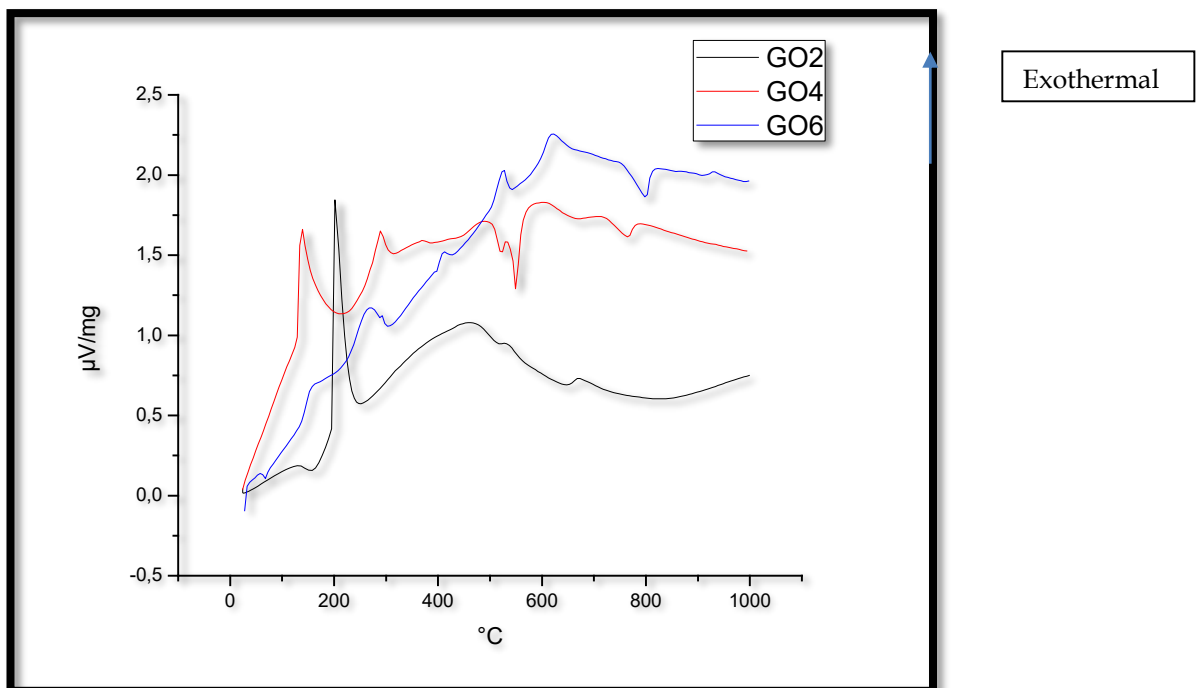


Figure 3.3: DTA Analysis of Zn-Fe co-doped HAP solution.

Fig. 3.2 represents mass change with temperature increase (TG) of HAP powder samples doped with different Fe and Zn proportions (GO2: 0,001 mole Fe-Zn doped HAp, GO4: 0,002 mole mole Fe-Zn doped Hap and GO6: 0,003 mole mole Fe-Zn doped Hap) and Fig.3.3 represents decomposition and crystallization ranges of powder.

Fig. 3.3 indicates loss-weight between 25°C-800°C. The reason of weight losses between 25°C- 250°C are based on the removal of free water and hydroxyl ions ( $\text{OH}^-$ ), between 250°C- 450°C the removal of nitrate ions ( $\text{NO}_3^-$ ) and between 450°C- 800°C the removal of carbonate ions ( $\text{CO}_3^{2-}$ ).

In the graphs it was also seen that, HAP was formed in monoclinic structure at a temperature of 200°C. And in between 600-800°C, the doped hexagonal HAP phase is stable due to the no weight-loss. The  $\beta$ -TCP phase has started to form at 800°C and this phase is stable at higher temperatures.

According to the Fig. 3.3 exothermic peaks created due to respectively decomposition of moisture, nitrate and carbonate groups from the system. Exothermic peaks in between 600-800°C represent crystallization of Fe-Zn co-doped HAP powder. During crystallization, HAP turns into  $\beta$ -TCP crystalline at nearly 680°C. Both graphs show that Fe-Zn doped Hydroxyapatite powder stays in stable formation without phase separation at low temperatures.

### 3.3. Thin Film Microstructure Analysis-X-RAY DIFFRACTION (XRD)

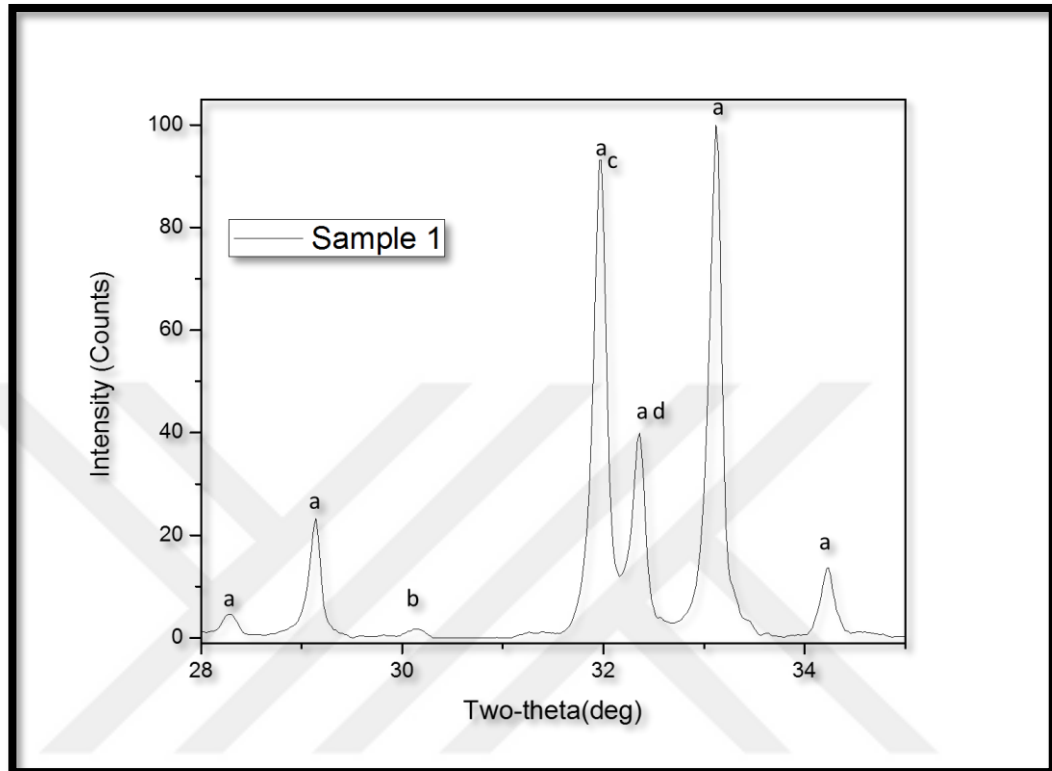


Figure 3.4: XRD Analysis of 0,0005 mole Zn-Fe doped HAP thin film.



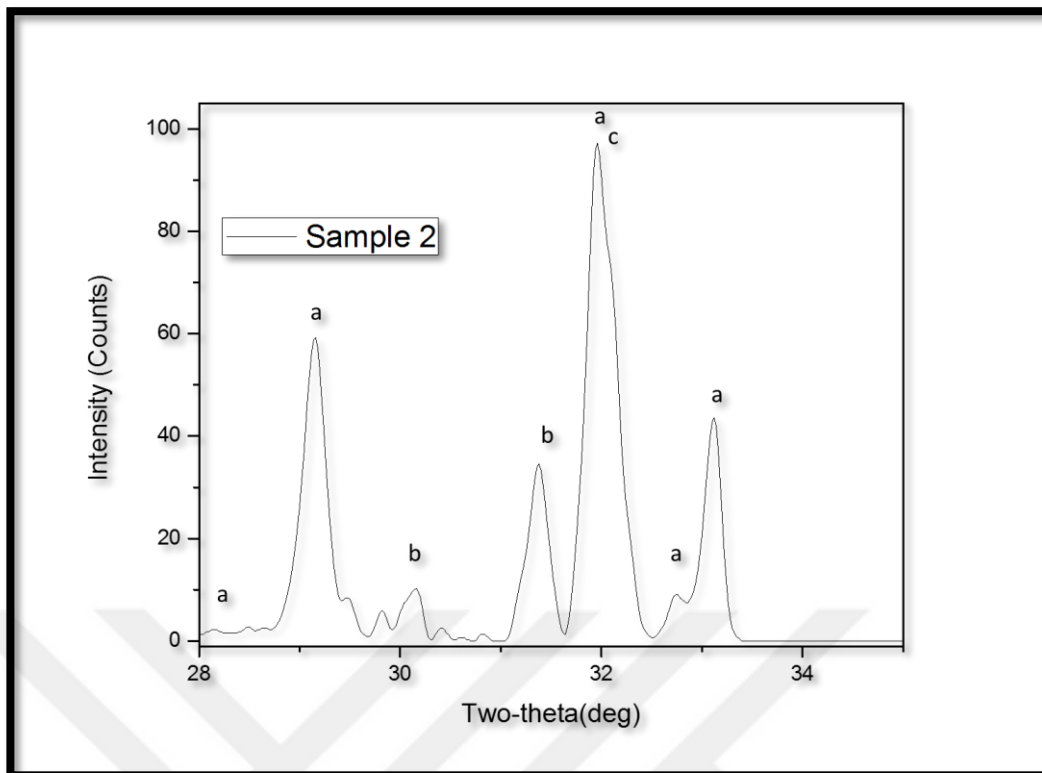


Figure 3.5: XRD Analysis of 0,001 mole Zn-Fe doped HAP thin film.

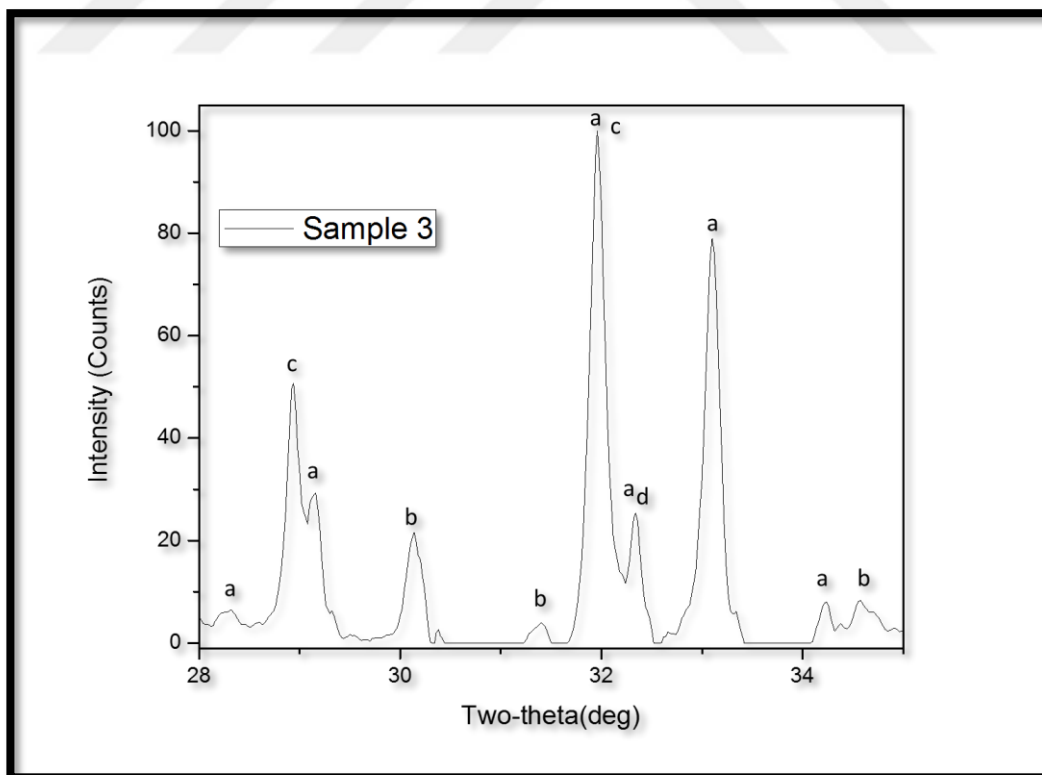


Figure 3.6: XRD Analysis of 0,0015 mole Zn-Fe doped HAP thin film.

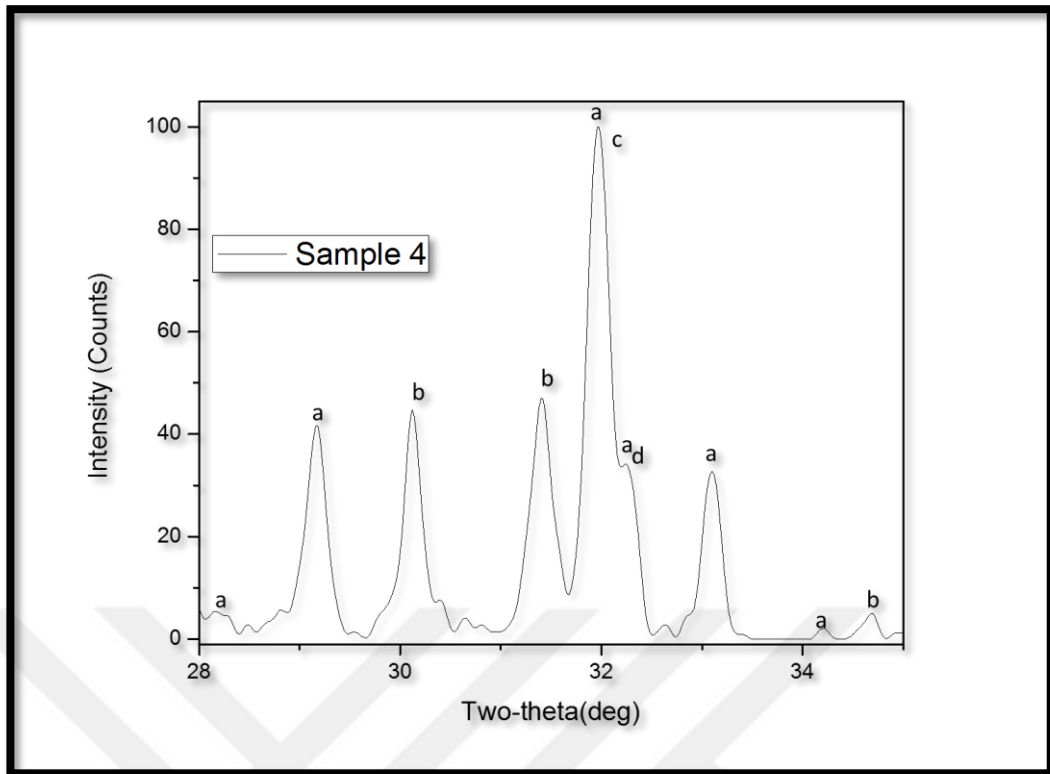


Figure 3.7: XRD Analysis of 0,002 mole Zn-Fe doped HAP thin film.

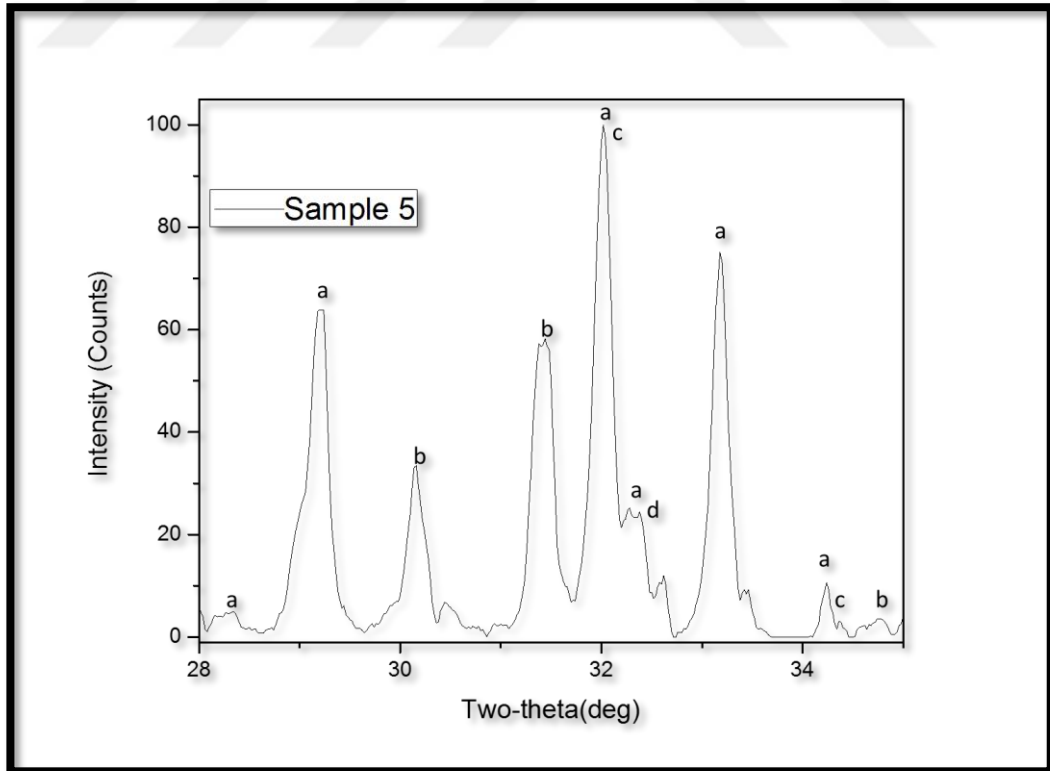


Figure 3.8: XRD Analysis of 0,0025 mole Zn-Fe doped HAP thin film.

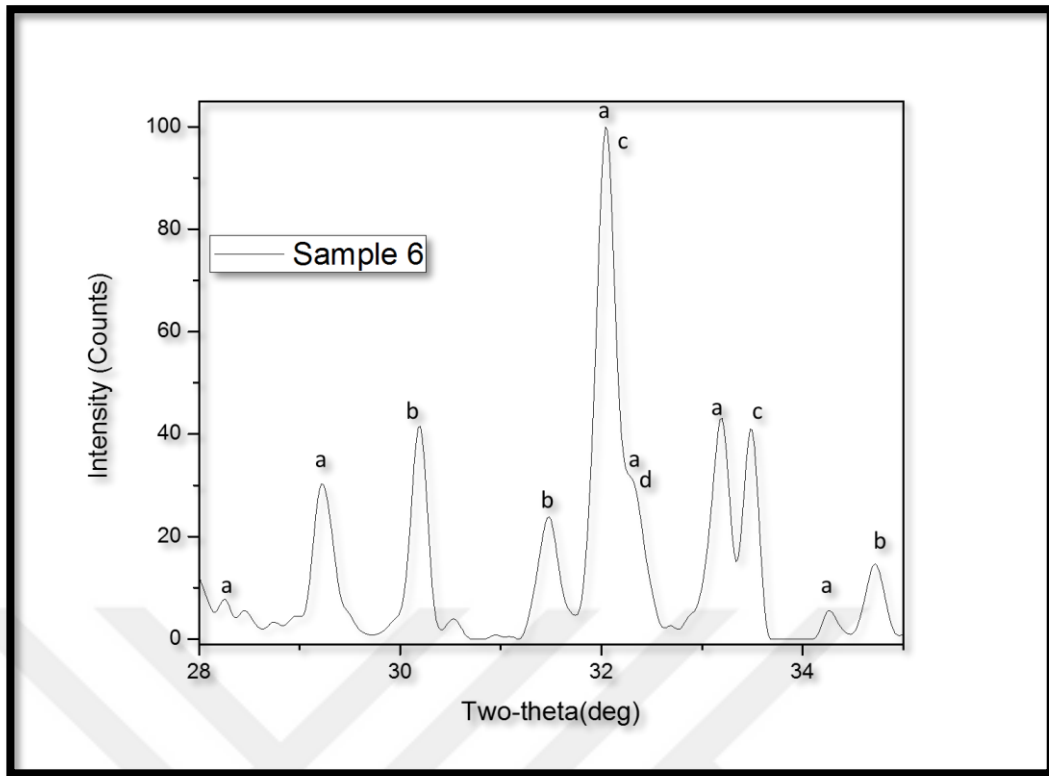


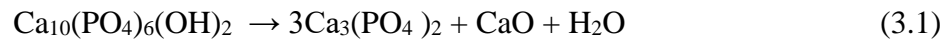
Figure 3.9: XRD Analysis of 0,003 mole Zn-Fe doped HAP thin film (a: HAP, b:  $\beta$ -TCP (Whitlocite), c: ZnO, d: CaO)

Table 3.4, 3.5, 3.6, 3.7, 3.8, 3.9 represent Zinc and Iron co-doped HAP thin films XRD analysis in various amounts.

In the analysis,  $\beta$ -TCP, CaO and ZnO phases and hexagonal HAP indexes in the all diffraction peaks being observed in  $2\theta$ : 28-35 degree with 0,1 mm/min speed.

In the XRD results of all samples HAP ((PDF 00-009-0432, P63/m (176))) phase was observed. As the amount of additive increases, the intensity of the peaks decreases, no expanding and shifting of the peaks were observed. It is understood that HAP crystal dimensions decrease with increasing amount of additive. On the other hand, it is observed that the peaks of the  $\beta$ -TCP ((PDF 01-070-2065), R-3c (167)) phase as well as the CaO ((PDF 01-082-1690), Fm-3m (225)) and ZnO ((PDF 01-075-1526), P63mc (186)) phases are becoming more evident with increasing amount of additives. HAP is unstable at temperatures above 800°C. It is understood that HAP crystal sizes are reduced as HAP starts to change into  $\beta$ -TCP above this temperature. Although the additive ions in these samples were dissolved in the HAP

phase, the reason for the CaO phase was observed in the environment was that HAP phase is converted to  $\beta$ -TCP phase at temperatures above 800°C.



The conversion of HAP to the  $\beta$ -TCP phase is given in Equation (3.1). As shown here, 1 mole of HAP phase is converted to 3 moles of  $\beta$ -TCP phase and 1 mole of CaO phase is formed.

Pure  $\beta$ -TCP cannot be obtained with aqueous solutions as it is not seen in biological systems but can be obtained at temperatures above 800°C. This temperature can be reduced by dissolving other ions in the  $\beta$ -TCP phase. In the  $\beta$ -TCP crystal, there are ion voids where ions smaller than  $\text{Ca}^{2+}$  ion diameter can settle. In an earlier study,  $\text{Ca}_{3-x}\text{Mg}_x(\text{PO}_4)_2$  phase which is more stable than  $\beta$ -TCP phase was obtained by using  $\text{Mg}^{2+}$  ion (S. Dorozhkin, "Calcium orthophosphates", *J.Mater. Sci.*, 42 (4): 1061-1095,2007.). In this study, it is thought that  $\text{Ca}_{3-x}\text{Fe}_x(\text{PO}_4)_2$  phase which is more stable than  $\beta$ -TCP phase is obtained. Because the heat treatment temperature was 1000°C for all samples, the  $\beta$ -TCP phase became more pronounced with increasing additive amount. This can be explained by the increase in the amount of additive, which reduces the crystallization temperature of the  $\beta$ -TCP phase and the formation of larger crystals in the heat treatment at 1000°C compared to the low doped  $\beta$ -TCP phase. Besides, the increment of additives proves that doping took place and Fe-Zn ions have tendency for Ca ions.

### 3.4. EDS Analysis

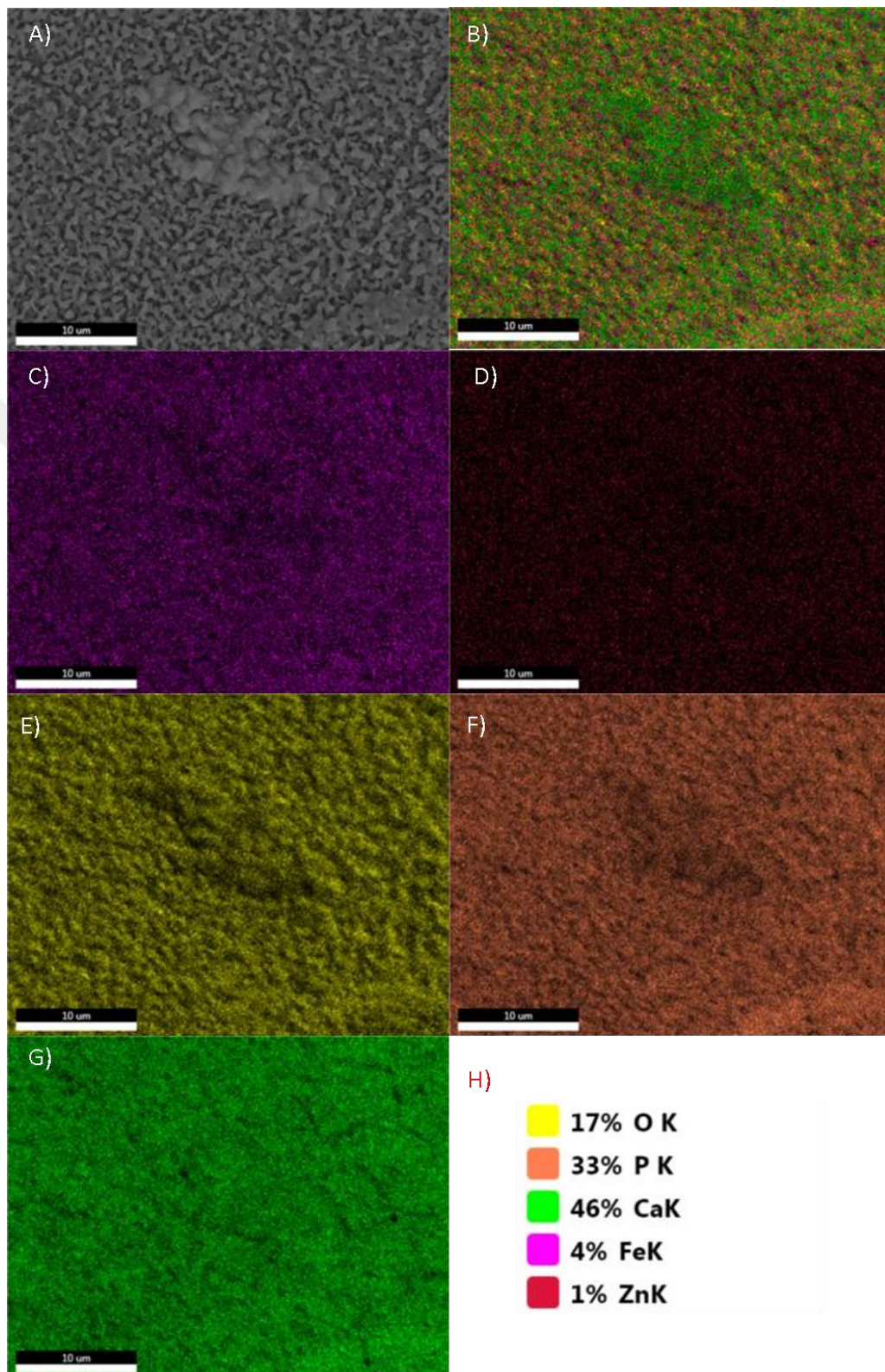


Figure 3.10: Atomic dispersion of 0,0025 mole doped Zn-Fe co-doped thin film.

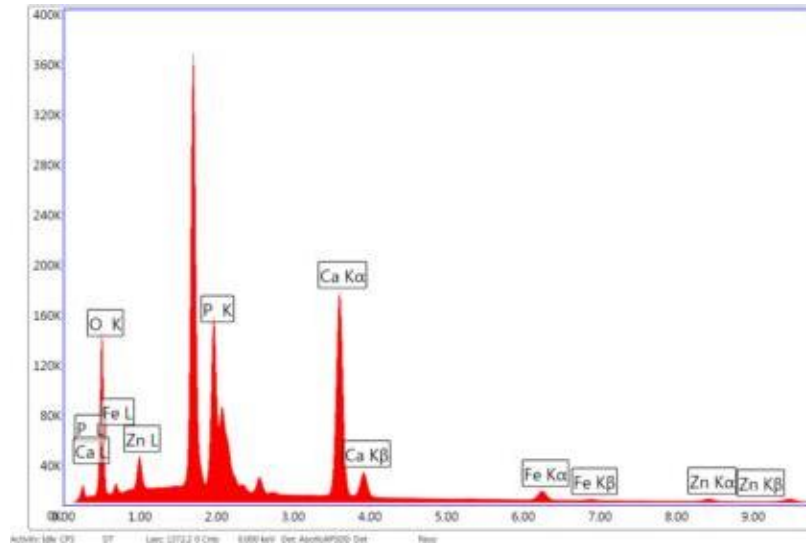


Figure 3.11: Net intensity of 0,0025 mole doped Zn-Fe co-doped thin film.

Table 3.1: Elemental analysis of 0,0025 mole doped Zn-Fe co-doped thin film.

Element	Weight %	Atomic %	Net Int.
O K	40.45	62.45	593
P K	15.77	12.58	1077.9
CaK	33.89	20.89	1339.9
FeK	5.28	2.33	74.6
ZnK	4.61	1.74	22.9

Weight and net intensity of 0,0025 mole doped thin film displayed by EDS measurement in Fig.3.10, 3.11, and Table 3.1. A represents normal image, B represents atomic dispersion of normal image specified with colors, C, D, E and F represent phase dispersions of Oxygen, Phosphate, Calcium and Iron phases. According to the percentage of Calcium is the most dominant and Phosphate ratio is second dominant. Due to  $Ca^{+2}$  and phosphate atomic percentage ratio, the  $Ca^{+2}/P$  value is 1,66. With reference to that, the dispersions of Calcium and Phosphate supports the idea that surface is coated via HAP and the lack of mound and roughness on the surface proves that HAP phase is intense. In the Figure it can also be seen that there occurs a phase on the image surface which can be recognize due to its color which is green stable and demonstrates  $\beta$ -TCP. In conclusion, HAP phase has the biggest surface area. Then  $\beta$ -TCP phase can come as a second phase and CaO phase have low activity and morphology difference is low.

### 3.5. SEM Analysis and Biocompatibility

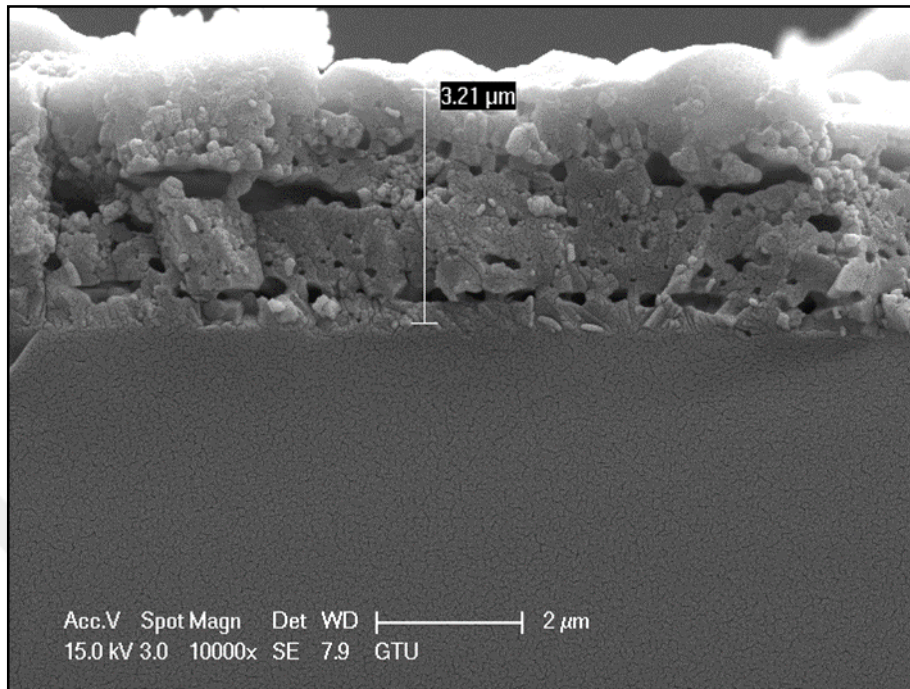


Figure 3.12: 0,0005 mole Zn-Fe co-doped HAP thickness measurement.

The Fig.3.12 shows thickness measurement of 20 times coated, Zn-Fe co-doped HAP thin film. 1nm- 5μm thickness accepted as ideal for coating to have a thin film feature and produced thin film thickness measured as 3,21μm.

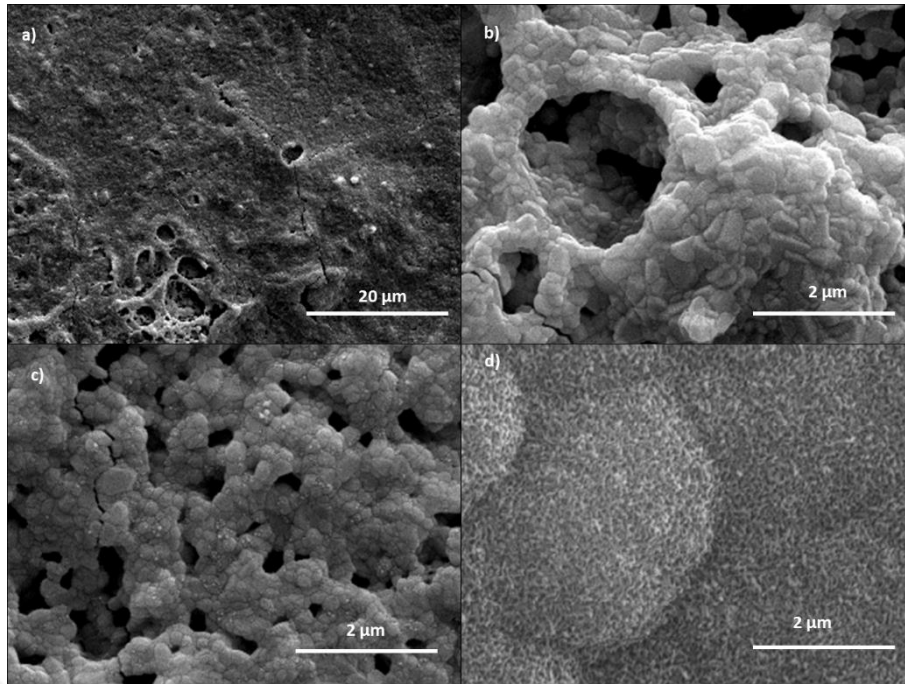


Figure 3.13: 0,0005 mole Zn-Fe co-doped HAP thin film SEM images, a)At low magnification, b) At high magnification, c)In SBF for 15 days, d)In SBF for 30 days.

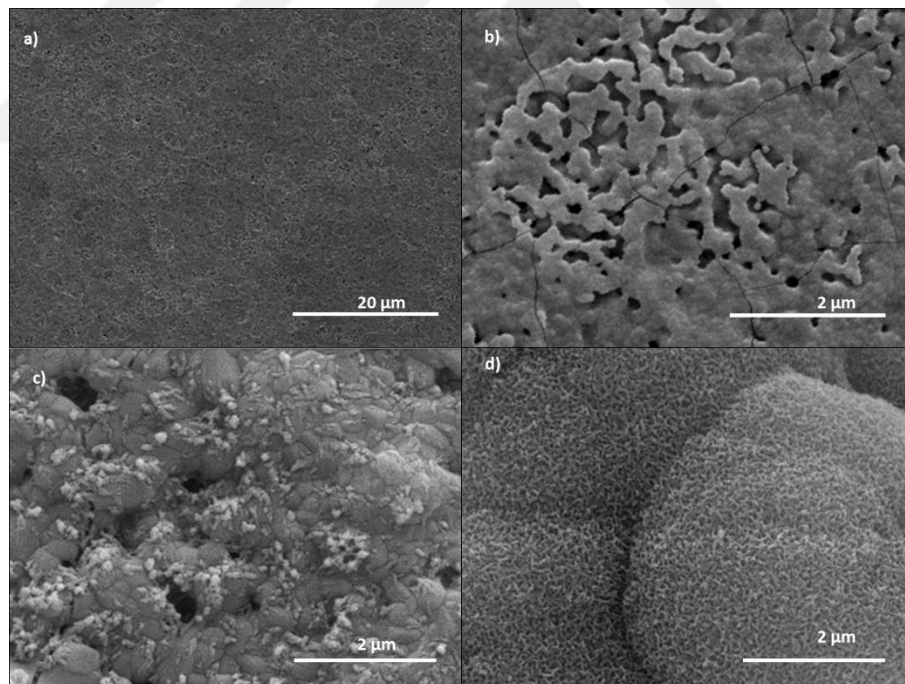


Figure 3.14: 0,001 mole Zn-Fe co-doped HAP thin film SEM images, a)At low magnification, b) At high magnification, c)In SBF for 15 days, d)In SBF for 30 days.



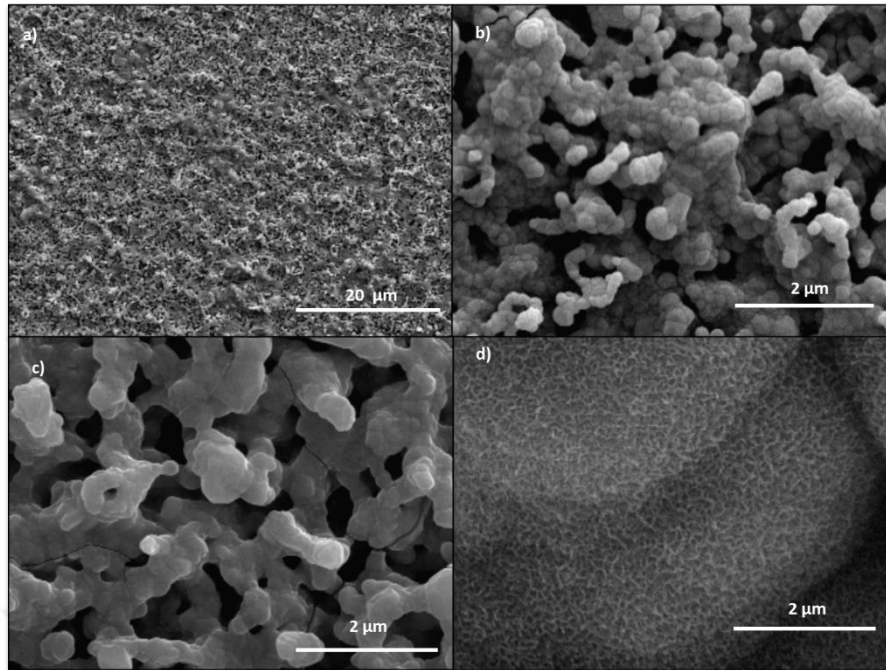


Figure 3.15: 0,0015 mole Zn-Fe co-doped HAP thin film SEM images, a)At low magnification, b) At high magnification, c)In SBF for 15 days, d)In SBF for 30 days.

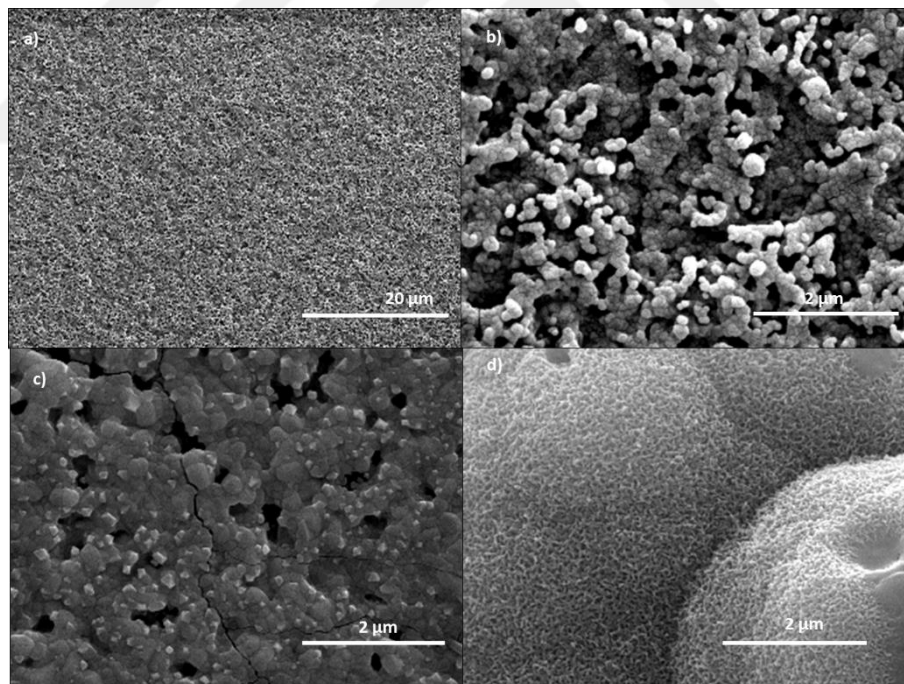


Figure 3.16: 0,002 mole Zn-Fe co-doped HAP thin film SEM images, a)At low magnification, b) At high magnification, c)In SBF for 15 days, d)In SBF for 30 days.

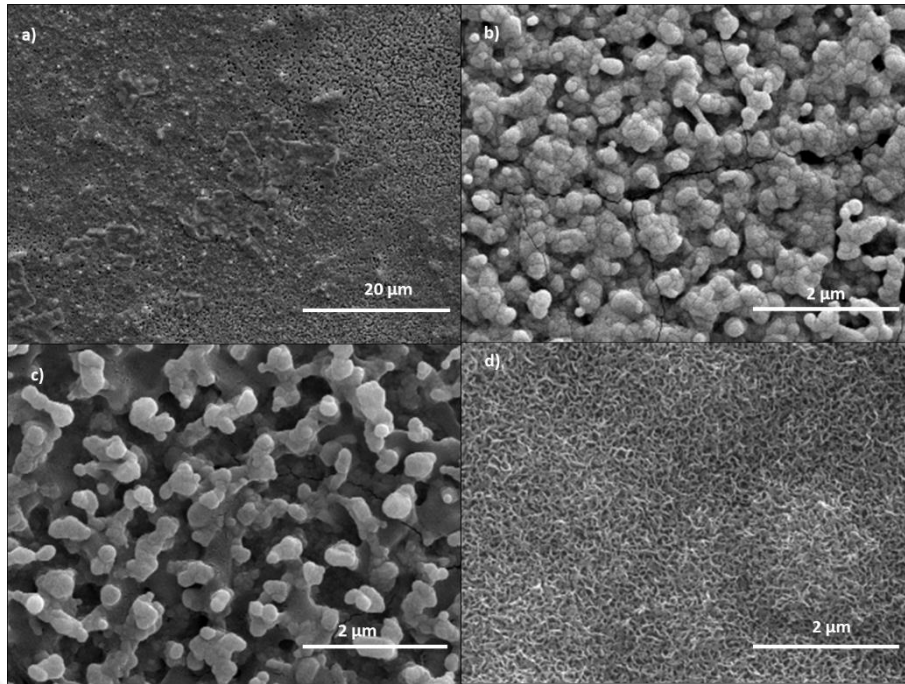


Figure 3.17: 0,0025 mole Zn-Fe co-doped HAP thin film SEM images, a) At low magnification, b) At high magnification, c) In SBF for 15 days, d) In SBF for 30 days.

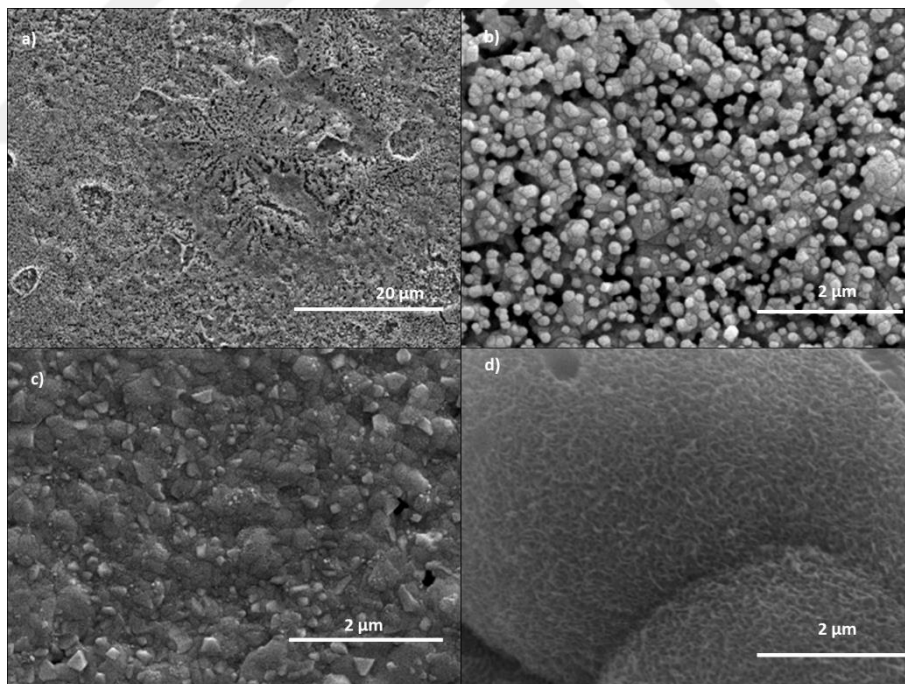


Figure 3.18: 0,003 mole Zn-Fe co-doped HAP thin film SEM images, a) At low magnification, b) At high magnification, c) In SBF for 15 days, d) In SBF for 30 days.

From Fig.3.12 to 3.18 at high magnification and low magnification enlarged SEM images of Zn-Fe co-doped HAP thin films were given respectively as 0,0005%, 0,001%, 0,0015%, 0,0020%, 0,0025% and 0,0030%. Below images which

were named as C and D are the results of after the samples immersed into SBF solution to observe the biocompatibility of the films.

In Figures the crack can be seen in low magnification images. These cracks formed because of the expansion coefficient of silicon wafer is bigger than produced Zn-Fe doped HAP thin films. Due to sudden decrease from 800°C to room temperature (25°C) during thin film production heat treatment for removal of organics causes these cracks. Furthermore, round protrusion during heat treatment can be interpreted as marks of outgassing on the surface. These structures increase surface area which are favorable.

In the figures it can be seen that the surface porosity of the thin films which were durated in SBF solution for 30 days was increased compared to 15 days duration. This porous apatite layer formed on the surface in SBF. It is an active structure that provides the connection between the doped thin film surface and the bone. In practice, this active structure accelerates the binding process between the actual bone and the doped HAP.

On the other hand, Ca, P and O elements as well as trace amounts of Fe and Zn elements were found in the EDS analysis of the regionally dense and partially porous film surfaces.

As with calcium phosphate, when a material is kept in SBF, a series of chemical reactions occur while the apatite layer forms on the surface. It is believed that the interface, surface chemistry, and even functional groups of materials in contact with the SBF play a very important role in the formation of bone ligaments. As it is known,  $\text{Ca}^{2+}$  element and  $\text{PO}_4^{3-}$  and  $\text{OH}^-$  groups are packed tightly in HAP structure. Where  $(\text{PO}_4)^{3-}$  and  $\text{OH}^-$  groups are negatively charged,  $\text{Ca}^{2+}$  ion is positively charged. The most negatively charged groups ( $(\text{PO}_4)^{3-}$  and  $\text{OH}^-$ ) play an active role during apatite formation on the material surface in SBS. While the material waits in SBF,  $\text{Ca}^{2+}$  ions in SBF adhere to  $(\text{PO}_4)^{3-}$  and  $\text{OH}^-$  ions on HAP surface with negative charge, as a result of this adherence, HAP surface has positive charge and  $(\text{PO}_4)^{3-}$  and  $\text{OH}^-$  negatively charged. As a result, apatite layer forms on the surface.

### 3.6. Antibacterial Test



Figure 3.19: Antibacterial test results of 0,0010 (GO1) and 0,0020 (GO5) and 0,0030 (GO6) mole Zn-Fe co-doped HAP pellets respectively.

Fig 3.19 represents the result image of antibacterial test after 1 week in bacteria medium. Black circles represent the area of pellets and the area between black and blue circles represents the area of antibiofilms.

In antibacterial test, Fe and Zn dopings comprise oxidation and reduction reactions due to the interaction of bacteria and the implants. In this interaction electron-hole transition and the antibacterial activity can be analyzed. The increment of antibacterial activity increases due to the interaction of oxygen and dehydrogenase enzymes. As a result of this interaction reactive oxygen carries the electrons and these electrons in conduction band turn into super oxide anions. Thereafter, the super oxide anions interact with  $H_2O$  then the hydrogen peroxide ( $H_2O_2$ ) and OH radicals are occurred as final products. On the other hand, the holes interact with absorbed

water molecules and form oxygen and OH radicals. This formation of radicals causes the bacteria cell deaths. Additionally, the high reduction effect of doping of  $\text{Fe}^{+3}$  and  $\text{Zn}^{2+}$  ions cause the oxidation in bacteria cell and cell membranes, which contain lipid and protein, by donating the electrons and devastate the cell membrane and cytoplasm.

In this figure the bacteria inhibition of Zn-Fe doped/undoped HAP pellets can be seen. According to the results the antibiofilm layer has the biggest surface area on GO6 (0,0030 mole Fe-Zn co-doped pellet) sample. Then undoped HAp, GO5 (0,0020 mole Fe-Zn co-doped pellet) and GO1 (0,0010 mole Fe-Zn co-doped pellet) samples have bigger antibiofilm area respectively. This proves that the Zn-Fe doped HAP has higher antibacterial features and the antimicrobial activity increases with the increment of additive amounts. In future researches the antibacterial efficiency can be increased by adding more dopants in HAP solution.

## 4. CONCLUSION

According to this study, Zn-Fe co-doped Hydroxyapatite thin films were produced successfully by dip-coating.

It was seen that the pellets obtained with / without HAP powders had an antimicrobial activity and as a result XRD, SEM and EDS analyzes were compatible with each other.

Similar to XRD analysis, HAP with large crystals initially decreases as the amount of additive increases, and on the contrary,  $\beta$ -TCP phase becomes more evident and HAP and  $\beta$ -TCP show similar behaviors in SEM analyzes. Since no particle size reduction or homogenization studies have been carried out, the particle size has varied in nm and  $\mu\text{m}$  scale.

XRD results showed that the HAP phase was present. It is understood that the amount of HAP crystal decreases with increasing amount of additive. On the other hand, it is observed that the peaks of the  $\beta$ -TCP phase as well as the CaO and ZnO phases are becoming more prominent with increasing amount of additive.

At temperatures above  $800^{\circ}\text{C}$  HAP is not stable and begins to convert to  $\beta$ -TCP, as the HAP crystal size is reduced.

In the SEM images, the surface of the sample shows a very dense and rough structure but some regions are porous. It is seen that the low amount doped HAP grains are larger, the grains in the structure are relatively more homogeneous, but as the amount of additives increases, the HAP grains shrink and the large grains re-form in the structure. This difference is thought to be due to the  $\beta$ -TCP phase.

In the EDS analysis, it is seen that the Ca/P atomic ratio is approximately 1.60. It is understood that there is no significant phase separation on the surfaces of the doped thin films. Again, it is seen that any element in the structure does not decompose clearly on the surface and is distributed homogeneously.

It was seen that apatite layer was formed on the sample surfaces which were kept in SBS for 15 and 30 days. A more porous layer of apatite was formed on the sample surfaces which were left for 30 days.

There is an observation in antimicrobial activity increment by adding  $\text{Zn}^{+2}$  and  $\text{Fe}^{+3}$  as dopants. And the increment of the additive amounts have positive effect on antibacterial test.

## REFERENCES

- [1] Bergmann, C., Stumpf A., (2013), “Dental Ceramics: Microstructure, Properties and Degredation”, 9-13, Springer-Verlag.
- [2] Güven, Ş., (2014), “Biyouyumluluk ve Biyomalzemelerin Seçimi”, Mühendislik Bilimleri ve Tasarım, 2, 303-311.
- [3] Zümrüt, Z., (2009), “Tam Faktöriyel Deney Tasarımı Tekniği ile Hidroksiapatit Kaplı Titanyum İmplant Malzemelerin Mekanik Özellikleri Üzerine Parametrelerin Etkisi”, Bitirme Tezi, İstanbul Teknik Üniversitesi.
- [4] Gümüşderelioğlu, M., (2002), “Biyomalzemeler” Bilim ve Teknik, 2 July.
- [5] Park, J., Lakes, R. S., (2007), “Biomaterials-An Introduction”, 3, Iowa: Springer.
- [6] Park, B. J., Bronzino, J.D., (2003), “Biomaterials principles and applications” Boca Raton: CRC Press.
- [7] Li, Y., Yang, C., Zhao, H., Qu, S., Li, X., Li, Y., 2014, “New developments of Ti- based alloys for biomedical applications”, Materials, 7, 1709-1800.
- [8] Geetha, M., Singh, A. K., Asokamani, R., Gogia, A. K., (2009), Ti based biomaterials, the ultimate choice for orthopaedic implants – A review. Progress in Materials Science, 54, 397–425.
- [9] Pasinli, A., (2004), “Biyomedikal uygulamalarda kullanılan biyomalzemeler”, Makine Teknolojileri Elektronik Dergisi, 4, 25-34.
- [10] Güven, S. Y. (2010) “Ortopedik malzemelerin biyouyumlulukları ve mekanik özelliklerine göre seçimi”, 2. Ulusal Tasarım İmalat ve Analiz Congress, 472-484.
- [11] Köktaş, S., (2015), “Ti6Al4V alaşımının içyapı ve yüzey özelliklerinin CaP bileşikleri ile doyurulmuş Mg içerikli MAO filmlerinin oluşumuna etkisi”, Yüksek Lisans Tezi, Dokuz Eylül Üniversitesi.
- [12] Mohammed T. M., Khana A.Z., Siddiquee A.N., (2012), “Titanium and its alloys, the imperative materials for biomedical applications”, International Conference on Recent Trends in Engineering and Technology, 91-95.
- [13] Chen, Q., Thouas, G. A., (2015), “Metallic implant biomaterials”, Materials Science and Engineering R, 87, 1–57.

- [14] Gonzalez, J. E. G., Mirza-Rosca, J. C., (1999), "Study of the corrosion behavior of titanium and some of its alloys for biomedical and dental implant applications", *Journal of Electroanalytical Chemistry*, 471, 109–115.
- [15] Lopez, M. F., Gutierrez, A. ve Jimenez, J. A., (2002), "In vitro corrosion behaviour of titanium alloys without vanadium", *Electrochimica Acta*, 47, 1359–1364.
- [16] Gür, A. K., Taşkın, M. (2004), "Metalik biyomalzemeler ve biyouyum" *Journal of Doğu Anadolu Bölgesi Araştırmaları*, 2, 106-13.
- [17] Pattanayak, D.K., Rao, B.T., Mohan, T.R.R., (2010), "Calcium phosphate bioceramics and bioceramic composites" *J. Sol-Gel Sci. Technol.*, 59(3), 432–447.
- [18] Sadat-Shojai, M., Khorasani, M.-T., Dinpanah-Khoshdargi, E., Jamshidi, A., (2013), "Synthesis methods for nanosized hydroxyapatite with diverse structures", *Acta Biomater.*, 9(8), 7591–7621.
- [19] Yang, Y.-C., Chen, C.-C., Wang, J.-B., Wang, Y.-C., Lin, F.-H., (2017), "Flame sprayed zinc doped hydroxyapatite coating with antibacterial and biocompatible properties" *Ceram. Int.*, 43 (Supplement 1), S829–S835.
- [20] Uskoković, V., Uskoković, D.P., (2011), "Nanosized hydroxyapatite and other calcium phosphates: Chemistry of formation and application as drug and gene delivery agents", *J. Biomed. Mater. Res. B Appl. Biomater.*, 96B(1), 152–191.
- [21] Zheng, B., Luo, Y., Liao, H., Zhang, C.,(2017), "Investigation of the crystallinity of suspension plasma sprayed hydroxyapatite coatings", *J. Eur. Ceram. Soc.*, 37(15), 5017–5021.
- [22] Kalita, S.J., Bhardwaj, A., Bhatt, H.A., (2007), "Nanocrystalline calcium phosphate ceramics in biomedical engineering", *Mater. Sci. Eng. C*, 27(3), 441–449.
- [23] Shepherd, J.H., Shepherd, D.V., Best, S.M., (2012), "Substituted hydroxyapatites for bone repair", *J. Mater. Sci. Mater. Med.*, 23(10), 2335–2347.
- [24] Habraken, W., Habibovic, P., Epple, M., Bohner, M., (2016), "Calcium phosphates in biomedical applications: materials for the future", *Mater. Today*, 19(2), 69–87.
- [25] Dorozhkin, S.V., (2010), "Bioceramics of calcium orthophosphates", *Biomaterials*, 31(7), 1465–1485.
- [26] Dorozhkin, S.V., (2016), "Multiphasic calcium orthophosphate (CaPO<sub>4</sub>) bioceramics and their biomedical applications", *Ceram. Int.*, 42(6), 6529–6554.



- [27] Bootchanont, A., Sailuam, W., Sutikulsoibat, S., Temprom, L., Chanlek, N., Kidkhunthod, P., Suwanna, P., Yimnirun, R., (2017), "Synchrotron X-ray Absorption Spectroscopy study of local structure in strontium-doped hydroxyapatite", *Ceram. Int.*, 43(14), 11023–11027.
- [28] Boanini, E., Gazzano, M., Bigi, A., (2010), "Ionic substitutions in calcium phosphates synthesized at low temperature", *Acta Biomater.*, 6(6), 1882–1894.
- [29] Eliaz, N., Metoki, N., (2017), "Calcium Phosphate Bioceramics: A Review of Their History, Structure, Properties, Coating Technologies and Biomedical Applications", *Materials*, 10(4), 334.
- [30] Chow, L.C., (2009), "Next generation calcium phosphate-based biomaterials", *Dent. Mater. J.*, 28(1), 1–10.
- [31] Dorozhkin, S.V., (2013), "Self-Setting Calcium Orthophosphate Formulations", *J. Funct. Biomater.*, 4(4), 209–311.
- [32] Pierre A.C., (1998), "Introduction to Sol-Jel Processing", Kluwer Academic Publishers.
- [33] Lin Y.S., Deng S.G., (1999), "Sol-Gel Preparation of Nanostructured Absorbents" *Surface Science and Catalysis*, 120(1), 653-686.
- [34] Şam E.D., (2001), "Çamların Sol-Jel Yöntemiyle Silika (SiO<sub>2</sub>) Kaplanması", Yüksek Lisans Tezi, İstanbul Teknik Üniversitesi, 137.
- [35] Asiltürk M., (2007), "Metal Alkoksit Temelli Kompozit Materyal Sentezi ve Boya Adsorpsiyonunda Kullanımı" Doktora Tezi.
- [36] Brinker C.J., Scherer G.W., (1989), "Sol-Jel Science", Academic Press, NY USA, 1.
- [37] Niederberger M., Pinna N., (2013), "Metal Oxide Nanoparticles in Organic Solvents; Synthesis, Formation, Assembly and Application", Springer, 978, 671-677.
- [38] Lev O., Wu Z., Bharathi S., Glezer V., Modestov A., Gun J., Rabinovic L., Sampath S., (1997), "Sol-gel Materials in Electrochemistry", *Chemical Materials*, 9, 2354- 2375.
- [39] Sayılkan F., (2003), "Organik Kirliliği Önlemede Kullanılabilecek Adsorban Sentezi ve Uygulanması", Yüksek Lisans Tezi, İnönü Üniversitesi.
- [40] Sayılkan H., (1992), "Sol-jel Prosesinin Ti, Zr ve Al Alkolatlarına Uygulanması ve Oluşan Ürünlerin Yapısının Aydınlatılması" Doktora Tezi, İnönü Üniversitesi.
- [41] Şam E. D., (2014), "Fonksiyonel Yüzeyler Ders Notları", Bursa Teknik Üniversitesi.

- [42] Collinson M. M., (1998), "Analytical Applications of Organically Modified Silicates", *Microchim. Acta.*, 129, 149-165.
- [43] Shaw D., (1992), "Introduction to Colloid and Surface Chemistry", Elsevier Butterworth Heinemann.
- [44] Turova N., (2002), "Chemistry of Metal Alkoxides", Hingham, Kluwer Academic Publishers, 37-68.
- [45] Mitzi D., (2009), "Solution Processing of Inorganic Materials" Hoboken, Wiley & Sons, 77-104.
- [46] Saka S., (1994), "Preparation and Properties of Sol-gel Coating Films", *Journal of Sol-gel Science and Technology*, 2, 451-455.
- [47] Roe B., Zhang X., (2009), "Durable Hydrophobic Textile Fabric Finishing Using Silica Nanoparticles and Mixed Silanes", *Textile Research Journal*, 79, 1115-1122.
- [48] Menning M., Schmitt M., Schmidt H., (1997), "Synthesis of Ag Colloids in Sol-gel Derived SiO<sub>2</sub> Coatings on Glass" *Journal of Sol-gel Science and Technology*, 8, 1035-1042.
- [49] Dash S., Mishra S., Patel S., Mishra B. K., (2008), "Organically Modified Silica Synthesis and Applications due to its Surface Interaction with Organic Molecules", *Adv. Colloid Interface Sci.*, 140, 77-94. 138.
- [50] Haryadi H., (2005), "Porous Hybrid Organic Inorganic Silica Materials Preparation, Structural and Transport Properties", *Doktora Tezi*, The University of New South Wales.
- [51] Brinker C.J. and Scherer G.W., (1990), "Sol-Gel Science, the Physics and Chemistry of Solgel Processing, Academic Press.
- [52] Hench L.L., (1998), "Sol-Gel Silica: Properties, Processing and Technology Transfer", Noyes Publications, 8-70.
- [53] Milea C.A., Bogatu C., Duta A., (2011), "The Influence of Parameters in Silica Sol-Gel Process", *Bulletin of the Transilvania University of Braşov*, 1, 4(53), 59-66.
- [54] Musgo J., Echeverria J.C., Estella J., Laguna M., Garrido J.J., (2009), "Ammonia Catalyzed Silica Xerogels: Simultaneous Effects of pH, Synthesis Temperature and Ethanol: TeOS and Water: TEOS Molar Ratios on Textural and Structural Properties, Microporous and Mesoporous Materials", 118, 280-287.
- [55] Park S.K., Kim K.D., Kim H.T., (2002), "Preparation of Silica Nanoparticles: Determination of the Optimal Synthesis Conditions for Small and Uniform

- Particles”, *Colloids and Surfaces A: Physicochemical and Engineering Aspects*, 197, 425-791.
- [56] Raut H.K., Ganesh V.A., Nair A. S., Ramakrishna S., (2011), “Anti-reflective Coatings: A Critical”, In-depth Review, *Energy Environ. Sci*, 4, 3779-3804.
- [57] Reisfeld R. ve Jorgenson C.K., (1992), “Chemistry, Spectroscopy and Applications of SolGel Glasses”, Monograph Series Structure and Bonding, Vol. 77, Springer-Verlag.
- [58] Mahltig B., Haufe H., Bottcher H., (2005), “Functionalisation of Textiles by Inorganic Sol Gel Coatings”, *Journal of Materials Chemistry*.
- [59] Kishimoto T., Kozuka H., J. (2003), “Sol-gel preparation of TiO<sub>2</sub> ceramic coating films from aqueous solutions of titanium sulfate (IV) containing polyvinylpyrrolidone”, *Mater. Res.*, 18, 466-474.
- [60] Soltmann U., Raff J., Selenska-Pobell S., Matys S., Pompe W., Bottcher H., J. (2003), “Biosorption of Heavy Metals by Sol-Gel Immobilized *Bacillus sphaericus* Cells, Spores and S-Layers”, *SolGel Sci. Technol.*, 26, 1209-1212.
- [61] Francis L.F., (1999), “Sol-Gel Methods for Oxide Coatings, Intermetallic and Ceramic Coatings, Dekker.
- [62] Schubert U., Husing N., Lorenz A., (1995), “Hybrid Inorganic-Organic Materials by Sol-Gel Processing of Organofunctional Metal Alkoxides”, *Chem. Mater.*, 7, 2010-2027.
- [63] Bohmer M.R., Keursten T., J. (2000), “Incorporation of Pigments in TEOS Derived Matrices”, *Sol-Gel Sci. Technol.*, 19, 361-364.
- [64] Cao S., Wang J., Chen H., Chen D., (2011), “Progress of marine biofouling and antifouling technologies”, *Schmidt, Appl. Organomet. Chem.*, 15, 331-343. 139
- [65] Novak B.M., (1993),” Hybrid Nanocomposite Materials—between inorganic glasses and organic polymers”, *Advanced Materials*, 5, 422-432.
- [66] Wen J., Wilkes G.L., (1996), “Organic/Inorganic Hybrid Network Materials by the Sol–Gel Approach”, *Chemical Materials*, 8, 1667-1681.
- [67] Pomogailo A.D., *Usp. Khim.*, (2000) “Hybrid polymer-inorganic nanocomposites”, *Russian Chemical Reviews*, 69, 60-89.
- [68] Dunn B., Zink J.I., J. (1991), “Optical properties of sol–gel glasses doped with organic molecules”, *Mater. Chem.*, 1, 903-913.
- [69] Avnir D., *Acc.* (1995), “Organic Chemistry within Ceramic Matrixes: Doped Sol-Gel Materials”, *Chem. Res.*, 28, 328-334.

- [70] Reisfeld R., (2001), "Prospects of sol-gel technology towards luminescent materials" *Opt. Mater.*, 16, 1-7.
- [71] Mennig M., Schmitt M., Schmidt H., J. (1997), "Synthesis of Ag-Colloids in Sol-Gel Derived SiO<sub>2</sub>-Coatings on Glass", *Sol-Gel Sci. Technol.*, 1997, 8, 1035-1042.
- [72] Weiping C., Lide C., J., (1997), "Synthesis and structural and optical properties of mesoporous silica containing silver nanoparticles", *Phys.: Condens. Matter*, 9, 7257-7267.
- [73] De G., J. (1998), "Sol-gel synthesis of metal nanoclusters-silica composite films", *Sol-Gel Sci. Technol.*, 11, 289-298.
- [74] Prokopenko V.B., Gurin V.S., Alexeenko A.S., Kulikauskas V.S., Kovalenko D.L., J. (2000), *Phys. D: Appl. Phys.*, 33, 3152-3155.
- [75] Carturan G., Campostrini R., Dire S., Scardi V., De Alteris D., *J. Mol. Catal.*, 1989, 57, 13-16.
- [76] Avnir D., Braun S., Lev O., Ottolenghi M., (1994), "Enzymes and Other Proteins Entrapped in Sol-Gel Materials", *Chem. Mater.*, 6, 1605-1614.
- [77] Zink J. I., Valentine J. S., Dunn B., New J. (1994), "Functional Hybrid Materials", *Chem.*, 1994, 18, 1109-1115.
- [78] Gill I., Ballesteros A., (1998), "Encapsulation of biologicals within silicate, siloxane, and hybrid sol-gel polymers: an efficient and generic approach" *Journal of American Chemical Society*, 120, 8587-8598.
- [79] Bottcher H., (2000), "Bioactive Sol-Gel Coatings", *Prakt Journal of Chemistry*, 342, 427-436.
- [80] Gill I., (2001), "Bio-doped nanocomposite polymers: Sol gel bioencapsulates", *Chemistry of Materials*, 13, 3404-3421.
- [81] Livage J., Coradin T., Roux C., J., (2001), "Encapsulation of biomolecules in silica gels", *Phys.: Condens. Matter.*, 13, 673-691.
- [82] Toprakdöşlü S., (2013), "Sol Jel Yöntemiyle TiO<sub>2</sub> Kaplanmış Paslanmaz Çelik Elektrotla Üzerindeki Poli(Anilin-Ko-İndol) Filminin Elektrokimyasal Davranışları", Doktora Tezi, Çukurova Üniversitesi.
- [83] Arslan A., (2010), "Sol-Jel Yöntemiyle Büyütülen Kalay Oksit Filmlerin Elektriksel ve Optiksel Özelliklerinin İncelenmesi" Yüksek Lisans Tezi, Ankara Üniversitesi.
- [84] Bardakçı, S., (2007), "Sol-jel Yöntemi İle Hazırlanan TiO<sub>2</sub> İnce Filmleri Optik Özelliklerinin Belirlenmesi", Yüksek Lisans Tezi, Sakarya Üniversitesi.

- [85] Karakız M., (2008), “Farklı Çözeltiler Kullanılarak Üretilen ZnO İnce Filmlerin Yapısal ve Optik Özelliklerinin İncelenmesi”, Kırıkkale Üniversitesi.
- [86] Parmod S., Shishodia P.K., Mehra R.M., (2007), “Influence of pH Value on the Quality of Sol-gel Derived ZnO Films”, *Applied Surface Science*, 253, 12, 5419-5424.
- [87] Vigneshwaran N, Kumar S., Kathe A.A., Varadarajan P.V., Parasad V., (2006), “Functional Finishing of Cotton Fabrics Using Zinc Oxide Soluble Nanocomposite”, *Nanotechnology*, 17, 5087-5095.
- [88] Yadav A., Parasad V., Kathe A.A., Ray S., Yadav V., Vigneshwaran N., (2006), “Functional Finishing in Cotton Fabrics Using Zinc Oxide Nanoparticles”, *Bull Mater.Sci.*, 29, 641-645.
- [89] Deng B.Y., Wei Q.F., Gao W.D., (2007), “AFM Characterization of Nonwoven Material Functionalized by ZnO Sputter Coating”, *Materials Characterization*, 58, 854-858.
- [90] Xu B., Cai Z., (2008), “Fabrication of a Superhydrophobic ZnO Nanorod Array Film on Cotton Fabrics via a Wet Chemical Route and Hydrophobic Modification”, *Applied Surface Science*, 254(18), 5899- 5904.
- [91] Xu B., Cai Z., Wang W., Ge F., (2006), “Preparation of Superhydrophobic Cotton Fabrics Based on SiO<sub>2</sub> Nanoparticles and ZnO Nanorod Arrays with Subsequent Hydrophobic Modification”, *Surface & Coatings Technology*, 204, 1556-1561.
- [92] Perelshtein I., Applerot G., Perkas N., Wehrschetz-Sigl E., Hasmann A., Guebitz G.M., Gedanken A., (2009), “Antibacterial Properties of an In situ Generated and Simultaneously Deposited Nanocrystalline ZnO on Fabrics”, *ACS Applied Materials and Interfaces*, 1(2), 363-366.
- [93] Sawai J., Kawada E., Kanou F., Igarashi H., Hashimoto A., Kokugan T., Shimizu M., J. (1996), “Disinfection Treatment of Heated Scallop-Shell Powder on Biofilm of *Escherichia coli* ATCC 25922 Surrogated for *E. coli*”, *Chem. Eng. Japan*, 29, 627.
- [94] Ohira T., Yamamoto O., Iida Y., Nakagawa Z. E., J. (2003), “Kinetics activity of *Yersinia Intermedia* Against ZnO Nanoparticles Either Synergism Antibiotics by Double-Disc Synergy Test Method” *Mater. Sci. Mater. Med.*, 19, 1407.
- [95] Zhang L., Jiang Y., Ding Y., Daskalakis N., Jeuken L., Povey M., O'Neill A. J., York D. W., J. (2010), “Mechanistic investigation into antibacterial behavior of suspensions of ZnO nanoparticles against *E-coli*” *Nano Res.*, 12, 1625.
- [96] Adams L.K., Lyon D.Y., Alvarez P.J., (2006), “Comparative eco-toxicity of nanoscale TiO<sub>2</sub>, SiO<sub>2</sub>, and ZnO water suspensions”, *Water Res.*, 40, 3527.

- [97] Rajagopalan S., Koper O., Decker S., Klabunde K. J., (2002), "Nanocrystalline Metal Oxides as Destructive Adsorbents for Organophosphorus Compounds at Ambient Temperatures", *Chem. Eur. J.*, 8, 2602.
- [98] Wang R., Hashimoto K., Fujishima A., Chikuni M., Kojima E., Kitamura A., Shimohigoshi M., Watanabe T., (1997), "Light-induced amphiphilic surfaces", *Nature*, 388, 431.
- [99] Vigneshwaran N., Kumar S., Kathe A.A., Varadarajan P.V., Parasad V., (2006) "Functional Finishing of Cotton Fabrics Using Zinc Oxide Soluble Nanocomposite", *Nanotechnology*, 17, 5087-5095.
- [100] Yufeng Z., Xu X., Xu Z., Wang J., Cai H., (2017), "Development of Fe-Based Degradable Metallic Biomaterials", *Metallic Biomaterials*, 3-20.
- [101] He J., He F., Li D., Liu Y., Liu Y., Ye Y., Yin D., (2016), "Advances in Fe-based biodegradable metallic materials", *RSC Advances*, 114.
- [102] D. L. Shi, (2006), "Introduction to Biomaterials, Tsinghua University Press, World Scientific Publishing Co. Pte. Ltd.
- [103] Gristina A. G., (1987), "Biomaterials Centered Infection. Microbial Adhesion versus Tissue Integration", *Science*, 237, 1588-95.
- [104] Gristina A. G., Hobgood C. D., Barth E., Pulverer G., Quie P.G., Peters G. (1987), "in Pathogenesis and Clinical Significance of Coagulase-negative Staphylococci", *Science*, 7, 143-57.
- [105] Christensen G. D., Simpson W. A., (1985), "Beachey EH. in Bacterial Adhesion: Mechanisms and Physiological Significance", *Science*, 4, 279-305.
- [106] Gristina A. G., Costerton J. W., (1984), "Bacterial Adherence and the Glycocalyx and Their Role in Musculoskeletal Infection", *Orthopedic Clinics of North America.*, 15, 517-535.
- [107] Gristina A. G., Costerton J. W., Leake E., Kolkin J., Jon M. J., Wright M. J., (1981), "Bacteria and Their Relationship to Biomaterials", *Orthopaedic Transactions*, 5, 332. [22] Baier R. E., Meyer A. E., Natiella J. R., Natiella R. R., Carter J. M., (1984), "Surface Properties Determine Bioadhesive Outcomes: Methods and Results", *Journal of Biomedical Materials Research Part A.*, 18, 337-355.
- [108] Dankert J., Hogt A. H., Feijen J., (1986), "Biomedical Polymers: Bacterial Adhesion, Colonization, and Infection", *CRC Critical Reviews in Biocompatibility*, 2, 219-301.
- [109] Albektsson T., Arnebrandt T., Larsson K., Nylander T., Sennerby L., (1985), "In transactions of the 5th European Conference on Biomaterials", *Williams DF, Ed. Elsevier*, 151- 152, 10-13.

[110] Vasir J.K., Labhasetwar V., (2005), “Targeted drug delivery in cancer therapy”, *Technology in Cancer Research and Treatment*, 4(4), 363-374.

[111] Chien Y. W, Lin S. (2007) “Drug Delivery: Controlled Release”, *Encyclopedia of Pharmaceutical Technology Vol. I*, New York: Informa Healthcare USA, Inc, 1082-1103.



## **BIOGRAPHY**

Gözde Öcal was born in 07.03.1993 in Istanbul. In 2011 she had studied in Gebze Technical University, Material Science and Engineering Department and she graduated in 2015. In the same year she has started to the master programme in Gebze Technical University, Institute of Natural and Applied Science, Material Science and Engineering Department. During her study she has started working in Şişecam Automotive A.Ş. as Project Engineer in 2018. Since then she is still working in the same company.

